REPORT
doi:10.26443/seismica.v3i2.1179

Investigation of suspected Holocene fault scarp near Montréal, Québec: The first paleoseismic trench in eastern Canada

Aube Gourdeau [*1], **Veronica B. Prush** [2], **Christie D. Rowe** [1], **Claudine Nackers** [3], **Hannah Mark** [4], **Isabel Morris** [5], **Philippe Rosset** [6], **Michel Lamothe** [7], **Luc Chouinard** [6], **Matthew S. Tarling** [1]

[1]Department of Earth & Planetary Sciences, McGill University, Montréal, Qc, Canada H3A 0E8, [2]Earth and Environmental Science Department, New Mexico Institute of Mining and Technology, Socorro, NM, USA 87801, [3]Civil, Geological and Mining Engineering Department, Polytechnique Montreal, Montréal, Qc, Canada H3T 1J4, [4]Department of Geology & Geophysics, Woods Hole Oceanographic Institution, Woods Hole, MA, USA 02543, [5]Department of Civil and Environmental Engineering, New Mexico Institute of Mining and Technology, Socorro, NM, USA 87801, [6]Department of Civil Engineering, McGill University, Montréal, Qc, Canada, H3A 0C3, [7]Département des Sciences de la terre et de l'atmosphère, Université du Québec à Montréal, Montréal, Qc, Canada, H2X 3Y7

Author contributions: *Conceptualization*: Prush, Gourdeau, Rowe. *Methodology*: Nackers, Rosset, Mark, Morris, Tarling . *Formal Analysis*: Mark, Rosset, Morris. *Investigation*: Gourdeau, Prush, Rowe, Nackers, Lamothe, Tarling, Wang, Zhu, Chien, Takahashi, Saint-Denis. *Writing - draft*: Gourdeau, Rowe, Prush, Mark, Rosset, Morris. *Writing - Review & Editing*: Gourdeau, Prush, Rowe, Nackers, Morris, Mark, Rosset, Chouinard, Lamothe. *Visualization*: Gourdeau, Rowe, Mark, Rossett, Tarling, Morris. *Supervision*: Rowe. *Project administration*: Gourdeau, Rowe. *Funding acquisition*: Rowe, Gourdeau.

Abstract Québec has experienced historical damaging earthquakes in several seismic zones (e.g. 1732 M5.8 Montréal, 1663 M7 Charlevoix, 1935 M6.2 Témiscamingue). Despite a high seismicity rate, no surface-rupturing faults have been discovered due to a combination of dense vegetation cover, recent glaciation, sparse earthquake records, and low regional strain rates. We manually searched lidar-derived digital elevation models (DEMs) of the region to search for potential post-glacial surface-rupturing faults across southern Québec and identified a scarp ∼50 km north of Montréal. We performed three geophysical surveys (ground penetrating radar, depth estimates from ambient seismic noise, and refraction seismology) that revealed a buried scarp, confirmed with a <1 m-deep hand-dug test pit. These observations convinced us to excavate the first paleoseismic trench in Québec to test for the presence of a surface-rupturing fault in July 2023. We found a glacial diamict containing no signs of syn- or post-glacial deformation. In this paper, we present the observations that led to the identification of a scarp and hypothesized faulting. We highlight the importance of trenching to confirm recent fault scarps in challenging environments. We hope our study can be used to optimize future paleoseismic research in the province of Québec and similar intracratonic glaciated landscapes.

Résumé Le Québec se situe dans une région intraplaque sujette à de nombreux séismes ayant causés des dommages (e.g. 1732 M5.8 Montréal, 1663 M7 Charlevoix, 1935 M6.2 Témiscamingue). Malgré une activité sismique régulière, la végétation dense, la déglaciation récente, les données sismiques sporadiques et le rythme de déformation lent ne concourent pas à l'identification de failles actives au Québec. Plusieurs modèles numériques topographiques (MNT) dérivés d'imagerie lidar (2016) du sud de la province ont été examinés afin d'identifier des candidats de failles sismiques post-glaciaires atteignant la surface, et montrent clairement un escarpement situé à ∼50 km au Nord de Montréal. Trois méthodes géophysiques (géoradar, bruit ambiant sismique et réfraction sismique) ont été employées sur l'escarpement, qui montrent un décalage du socle rocheux à faible profondeur, confirmé par une première excavation de l'ordre de 1 m de profondeur. Ces observations ont justifié l'excavation en juillet 2023 de la première tranchée paléosismique effectuée au Québec, afin de confirmer la présence d'une faille sismique récente atteignant la surface. Cette tranchée révèle la présence d'un diamicton ne contenant aucun signe de déformation syn- ou post-glaciaire. Cet article présente les observations ayant faussement mené à l'identification d'un escarpement érosif comme étant une faille sismique. Il montre ainsi l'importance de réaliser des tranchées paléosismiques lors de l'identification de failles actives, spécialement dans des environnements complexes. Cette étude permettra d'optimiser les recherches à venir dans le domaine de la paléosismologie au Québec et dans des environnements intracratoniques au passé glaciaire.

Production Editor:
Gareth Funning
Handling Editor:
Ake Fagereng
Copy & Layout Editor:
Théa Ragon

Signed reviewer(s):
John Adams
Jack Williams

Received:
January 29, 2024
Accepted:
June 30, 2024
Published:
July 25, 2024

*Corresponding author: aubegourdeau@gmail.com

Non-technical summary The cities of Montréal, Ottawa, and Ville-Marie (Témiscamingue) lie within a zone of activity that has experienced historical damaging earthquakes (e.g. 1732 M5.8 Montréal, 1663 M7 Charlevoix, 1935 M6.2 Témiscamingue), but no seismic faults have been identified in the region. Due to dense vegetation cover and recent glaciation that eroded the surface, faults are difficult to observe in this landscape. We used elevation maps from lidar data to search for topographic evidence of faulting and identified a scarp ∼50 km north of Montréal. Three geophysical surveys revealed a buried bedrock offset that was confirmed with a <1 m-deep hand-dug test pit. These observations convinced us to excavate a trench across the scarp to test for evidence of sediment deformation and thus, faulting. We found glacial sediments containing no signs of deformation and concluded that the scarp was not formed by recent faulting. In this paper, we present the observations that led to the identification of a scarp and hypothesized faulting. We highlight the importance of trenching to confirm recent fault scarps in challenging environments. We hope our study can be used to optimize future research in paleoseismology in the province of Québec and similar recently deglaciated landscapes.

Résumé non technique Les villes de Montréal, Ottawa et Ville-Marie (Témiscamingue) se situent dans une zone d'activité sismique sujette à de nombreux séismes destructeurs (e.g. 1732 M5.8 Montréal, 1663 M7 Charlevoix, 1935 M6.2 Témiscamingue), mais aucune faille sismique n'a encore été identifié dans la région. La dernière glaciation, qui a érodé le territoire, et la végétation dense rendent la tâche ardue. Des cartes d'élévation lidar ont été utilisées afin d'identifier des changements abrupts et isolés de la topographie, potentiellement associés à des mouvements sismiques. Un escarpement bien individualisé a été observé à ∼50 km au nord de Montréal. Trois levés géophysiques et une excavation superficielle (1 m de profondeur) effectués sur le site ont permis de confirmer ce décalage du socle rocheux en profondeur. Ces observations ont poussé l'équipe à réaliser une tranchée plus importante contre le socle rocheux, l'objectif étant d'identifier si un déplacement des sédiments en profondeur est visible, ce qui prouverait l'activité d'une faille sismique. Les sédiments glaciaires dans la tranchée ne montrent aucun signe de déformation, ce qui invalide notre proposition de départ. Cet article présente les observations et mesures effectuées sur la faille identifiée en surface et souligne l'importance d'effectuer une tranchée lorsqu'une faille active est suspectée dans des environnements post-glaciaires et complexes. Cet article pourra aussi servir de guide afin d'optimiser les recherches en paléosismologie au Québec.

1 Introduction

Montréal lies within the western Québec Seismic Zone (WQSZ). The WQSZ is a region of elevated but poorly defined earthquake hazard which has experienced several historic, damaging earthquakes (Lamontagne, 2002; Ebel, 2011). In 1732, a M5.8 earthquake caused significant damage in the Montréal area, notably to chimneys, wells, and walls (Leblanc, 1981). Given the relatively large magnitude of this earthquake and other historic events in southern Québec (1935: M6.2, Témiscamingue; 1663: M7.5, Charlevoix), it is possible that some of these events could have produced surface ruptures (Leblanc, 1981; Brooks and Adams, 2020; Ebel, 2011; Lamontagne, 2002; Mérindol et al., 2022). However, despite these large earthquakes, no studies to date have identified active faults in the region (Brooks and Adams, 2020) and therefore observationally-constrained specific sources are not yet available to support ground motion models (e.g. Pagani et al., 2014). The 1989 M_s6.3 Ungava earthquake and resultant Lac Turquoise fault scarp is the first known surface-rupturing earthquake on the eastern margin of North America and the only one in Québec (Adams et al., 1991). Due to the lack of identified surface ruptures, a generalized region of elevated hazard appears in seismic hazard maps without any fault-specific sources or scenarios (Earthquakes Canada, 2020; Thompson Jobe et al., 2022). The complete instrumental record of historical M5+ seismicity for the Western Québec Seismic Zone dates back only to 1928, and pre-instrumental earthquake history is reconstructed by estimating shaking magnitude from witness accounts (Basham, 1982; Lamontagne et al., 2018), liquefaction records (e.g. Tuttle and Seeber, 1991; Tuttle and Atkinson, 2010) or landslides (Brooks and Perret, 2023), and lake sediment records (Doig, 1990; St-Onge et al., 2004) rather than assessing hazard through paleoseismic techniques such as fault trenching or geomorphic slip rate analyses.

Earthquake source faults are identified in seismically active regions by scarps and offset geomorphic features, precisely located microseismicity, and observations of surface rupture (McCalpin, 2009; Yu et al., 2016; Zielke et al., 2015). Until recently, topographic maps in the province of Québec were not available in sufficient resolution to delineate the subtle geomorphic features that might be formed during moderate earthquakes. In 2016, the Québec government released lidar-derived, high-resolution digital elevation models (DEMs) that cover most of the WQSZ and two major urban centers (Montréal and Québec City) (Ministère des Forêts, 2016). We manually surveyed these elevation models and identified several potential fault scarps offsetting ∼8-12 ka glaciomarine sediments (Globensky, 1987; Randour et al., 2020b,a; Gourdeau et al., 2023).

The young post-glacial surface history of Québec,

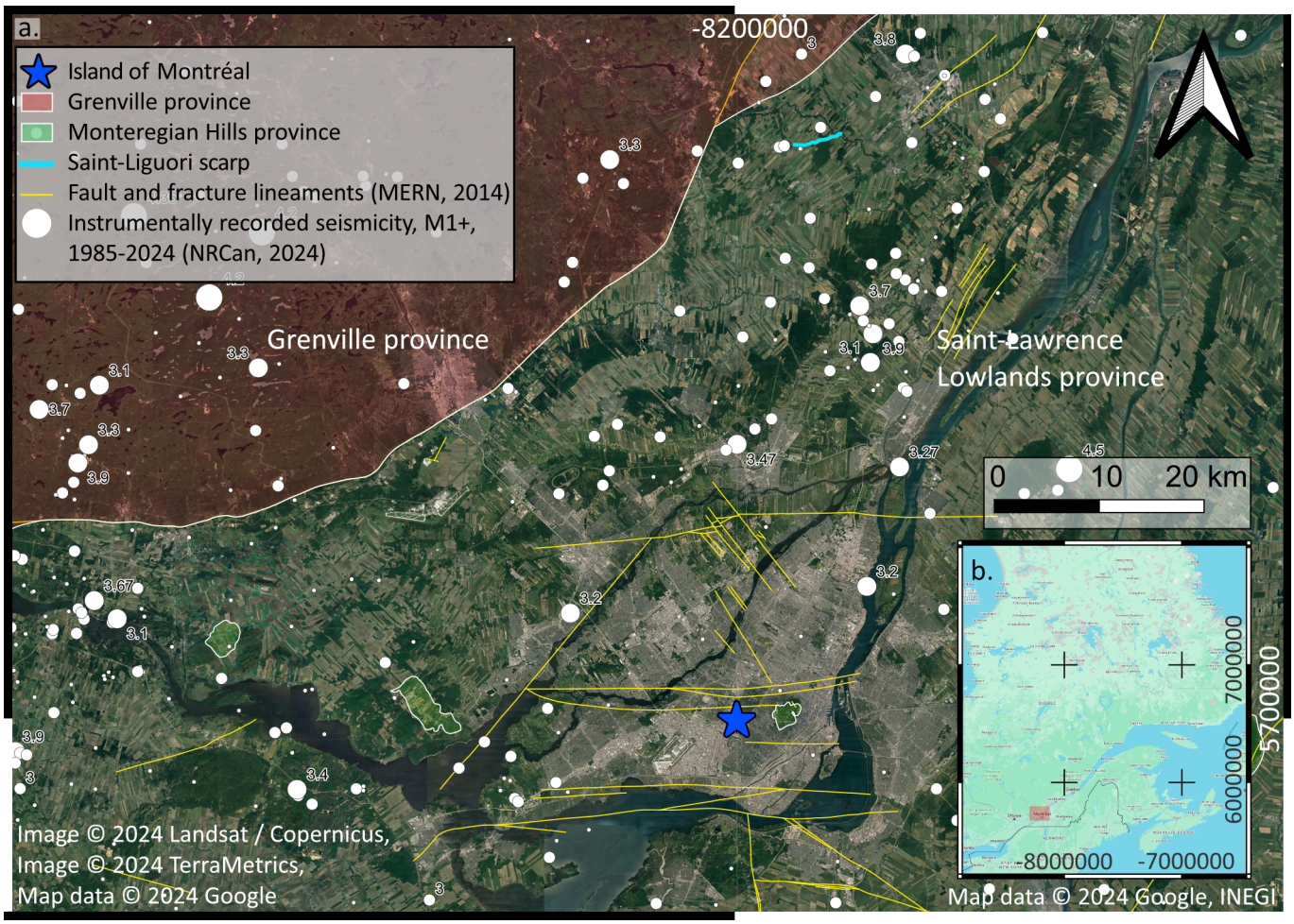

Figure 1 Map of the Saint-Liguori scarp (light blue), its distance from the Island of Montréal, and the instrumentally recorded seismicity in the area since 1985 (Natural Resources Canada, 2024); 2022 population 2,038,000 (Ministère de l'Économie, de l'Innovation et de l'Énergie, 2022). The basemap for the main figure is from © 2024 Landsat/Copernicus, © 2024 TerraMetrics, and © 2024 Google, and the basemap for the inset is from © 2024 Google, INEGI. a) General map of fault and fracture lineaments (yellow) by the Ministry of Energy and Natural Resources of Quebec (MERN) based on field observations made during cartographic surveys. b) Inset shows area of (a) in Québec in red box.
En français: Carte comprenant la position de l'escarpement de Saint-Liguori par rapport à l'île de Montréal et les séismes répertoriés à l'aide de sismomètres depuis 1985 (Natural Resources Canada, 2024); population de 2022 2,038,000 (Ministère de l'Économie, de l'Innovation et de l'Énergie, 2022).La carte de fond pour la figure principale provient de © 2024 Landsat/-Copernicus, © 2024 TerraMetrics, et © 2024 Google, et la carte de fond de l'encadré provient de © 2024 Google, INEGI. a) La carte générale des failles et fractures (jaune) a été créée par le Ministère de l'Énergie et des Ressources Naturelles (MERN) basée sur des observations faites lors de campagnes de cartographie. b) Carte montrant l'étendue de la carte (a) dans le sud du Québec.

coupled with regional low strain rates, means that if any surface-rupturing fault scarps exist we expect them to form low tectonic scarps and cumulative offset. One of the rare intracratonic analogs of Québec that has documented surface-rupturing, post-glacial fault scarps is Fennoscandia, where paleoseismic records have been studied in detail (Sutinen et al., 2014; Mikko et al., 2015; Smith et al., 2014; Palmu et al., 2015; Steffen et al., 2021a, part III). In glaciated environments, caution is required when studying scarps that could be associated with earthquakes. Erosion and enhancement of joints and fractures by ice plucking could form scarps during deglaciation that are not associated with seismicity, and other seismic features could have been eroded away by glacial advance and retreat. If surface processes outpace displacement, scarps don't develop strong geomorphic expressions (Cox et al., 2012). The spatiotemporal patterns of intraplate earthquakes are also poorly understood (Stein, 2007). For example, it is unknown whether individual faults have regular recurrence intervals or whether seismicity is chaotically distributed across a wide region of faults (Stein, 2007; Atkinson, 2007; Steffen et al., 2021b). Moreover, glaciotectonic features in tills can confound tectonic fracture identification (e.g. Pisarska-Jamroży et al., 2019). The development of conceptual frameworks for patterns of intraplate seismicity requires more data to understand how these seismic zones differ from active plate boundary environments.

In spite of these challenges, paleoseismic investigations in Fennoscandia have successfully recovered seismic history on low-strain rate faults in a similar set-

ting (e.g. Mörner et al., 2000; Markovaara-Koivisto et al., 2020). We assert that due to predictions of post-ice sheet flexure associated with lithospheric rebound (e.g. Lambeck et al., 2017; Godbout et al., 2023), similar field data is potentially recoverable in southern Québec. The main objective of this study was to demonstrate this feasibility by excavating the first paleoseismic trench in eastern Canada on a potential surface-rupturing fault scarp. Due to a lack of previous paleoseismic trenching in Québec, it took some time to develop an understanding of legal hurdles and professional cooperation necessary to pursue this research, so we document our experience here to aid future investigators working in Québec and eastern Canada. Our site specific health and safety plan (in French) is provided in the supplementary material for reference (See Section Data and code availability for links to all repositories.)

As part of a broader regional inventory (Gourdeau et al., 2023), we identified a possible fault scarp ~45 km NE of Montréal near the village of Saint-Liguori (Fig. 1), which we named the "Saint Liguori scarp". Given the proximity of this scarp to the city of Montréal, it was a priority target for further investigation. Here we report the geomorphic expression of the scarp in the context of the post-glacial evolution in the St. Lawrence Valley. We present three geophysical methods (ground penetrating radar, H/V ambient seismic noise, and seismic refraction tomography) used onsite to demonstrate a subsurface bedrock scarp, and document a preliminary test pit demonstrating deformed post-glacial sediments - bedrock contact which constitutes the proposed fault. We finally demonstrate how the results of each investigation was consistent with a recently active fault scarp until we dug a paleoseismic trench, which revealed no deformation. Our outcome demonstrates for the first time that paleoseismic trenching is possible and desirable in Québec. Trenches can provide valuable information on the glacial to post-glacial deposits that are critical for interpreting surface deformation evidence, especially in challenging and deglaciated environments. Moreover, trenching is crucial for identifying false-positives that were solely identified from geomorphic indicators.

2 Background

Approximately 90% of the bedrock of Québec is made of the Precambrian rocks of the Canadian shield, a cratonic setting (Hoque, 2014). The St. Lawrence river sits on the St. Lawrence platform of Cambrian-Ordovician age, preserved in the St. Lawrence aulacogen between the Grenville Orogenic belts to the north and northwest (Fig. 1a), and the Appalachian Mountains to the south and southwest (Tremblay et al., 2013). The elevated seismicity in the St. Lawrence region has been attributed to numerous causes, including lithospheric thinning and inherited crustal faults from Paleozoic orogenesis, Mesozoic rifting (Rimando and Peace, 2021), and Cretaceous hot spot activity (Ma and Eaton, 2007), on which a recent stress perturbation caused by post-glacial rebound is superimposed (Sella et al., 2007; Henton et al., 2006; Goudarzi, 2016). Rimando and Peace (2021) suggested that faults with NW strikes had the highest slip tendencies (inferred from recent earthquake focal mechanisms) across eastern Canada based on current regional stresses. Without more specific information about the evolution of stress directions since glacial recession, we did not narrow our search to NW-striking potential faults.

The St. Lawrence valley lies in a Paleozoic aulacogen which formed during the opening of the Iapetus (proto-Atlantic) ocean (Kumarapeli and Saull, 1966), and whose bounding faults have been reactivated several times, including during the Cretaceous (Tremblay et al., 2013). More recent reactivation of some scarps is possible, but not proven (e.g. Pinet et al., 2020) (Fig. 1). The bounding normal faults (similar to the contacts represented with white trace in Fig. 1 a) have cumulative throws of 2-3 km and parallel faults interpreted from seismic reflection profiles in the St. Lawrence Estuary have throws of hundreds of metres (Tremblay et al., 2013).

2.1 Glacial and post-glacial history of Québec

The Laurentide Ice Sheet (LIS) covered southern Québec ~21 ka ago during the Last Glacial Maximum (LGM) (Hoque, 2014; Dyke et al., 2002; Sella et al., 2007; Occhietti et al., 2011). This ice sheet was up to 4 km thick in central Québec, and the weight of the ice significantly depressed the crust in Canada (Walcott, 1972; Simon et al., 2016). Ice sheet retreat left behind depositional and erosional geomorphic features such as moraines, drumlins, eskers, erratics, glacial striations, and bedrock fractures (Bennett and Glasser, 2011; Occhietti et al., 2011). Marine incursion followed the melting of the ice sheet at about 11 ka BP, followed by recession as the continent rebounded (Occhietti and Richard, 2003; Richard and Occhietti, 2005). Isostatic rebound is still ongoing in southern Québec at a rate of ~3-5 mm/yr (Tarayoun et al., 2018).

This recent deglaciation strongly impacted the geomorphology of Québec and modified or erased evidence of scarps or offsets predating the marine incursion at ~13.1–12.8 ka (Cronin et al., 2008; Occhietti et al., 2011). Due to glaciation and post-glacial marine and lacustrine deposition, the land surface of southern Québec has been almost completely resurfaced or covered with thin Pleistocene-Holocene sediments (Occhietti et al., 2011). The maximum marine inundation in southern Québec and southeastern Ontario, associated with the lake Candona episode, is at a present-day elevation of about 230 m, and Pleistocene deposits can reach thicknesses >100 m (e.g. near Lac St-Pierre, Lamothe, 1993) (Occhietti et al., 2011). Near St-Liguori, the deposits are thin due to the presence of bedrock highs in the area. Any surface scarps developed by faulting during the early glacial recession may have been eroded at this time.

Consequently, the production of earthquake-related offsets in the province, if any, must have developed since the late Pleistocene, suggesting that any scarps found in the region must have developed very recently. In a low strain rate environment, this short time period for developing evidence of fault activity suggests that any fault-related features are expected to be small in

amplitude (Oliver et al., 1970; Mazzotti, 2007; Tarayoun et al., 2018).

2.2 Seismic history of greater Montréal area

There is reason to believe that Montréal faces a hazard of an ∼M6 or greater earthquake due to a historical estimated M5.8-6 event which struck the then very small settlement in 1732 (Leblanc, 1981; Rosset et al., 2021; Thompson Jobe et al., 2022). The paleoseismic record of southern Québec is sparse, but the identification of subaqueous debris flows, landslides, mass transport deposits, and liquefaction features in lacustrine and marine sediments have been suggested to record post-glacial shaking (Brooks and Adams, 2020). Based on global seismicity rates in stable cratons and the statistical calculations used by Fenton et al. (2006) in Ontario, Brooks and Adams (2020) estimated that 28-160 surface-rupturing earthquakes might have occurred in eastern Canada since the recession of the ice sheets. However, there are significant uncertainties around seismicity rates in intraplate regions (Stevens and Avouac, 2021; Iturrieta et al., 2024), and it is not yet possible to assess the geologic record since only a single fault scarp has been confirmed in the region (Adams et al., 1991; Brooks and Adams, 2020). Nevertheless, several of the historical earthquakes in Québec were large enough to potentially create surface ruptures. In addition to the 1732 earthquake in Montréal, other historical earthquakes big enough to have caused surface ruptures include the 1663 M7 Charlevoix earthquake and the 1935 M6.2 Témiscamingue earthquake (Leblanc, 1981; Lamontagne, 2002; Ebel, 2011). A cluster of seismicity has also been identified by (Chien and Liu, 2023) in the area of Joliette, about 60 km north-east of Montréal.

3 Geomorphic expression of the Saint-Liguori Scarp

Lidar-derived products, (DTM, slope, hillshade) made available by the Ministère des Forêts et des Parcs since 2016, were used in QGIS and ArcGIS and sometimes reconverted to different versions of hillshade images to evaluate the location of potential fault scarps. We commonly used a Z factor of 2 with the default settings chosen by the ministry, which represented an illumination angle of 315°N at an altitude of 45°. However, these parameters were sometimes changed to maximize visibility, contrast, and brightness.

Using these lidar-derived datasets, we applied a set of criteria for scarp identification adapted from methods used in Fennoscandia (Sutinen et al., 2014; Smith et al., 2014; Palmu et al., 2015; Mikko et al., 2015). Fault scarps and earthquake sources in Fennoscandia have been identified remotely by the observation of offset of drainage networks (either displacement of previously established channels or channel deflections recording apparent accommodation of baseline changes associated with fault throw), along-strike continuity and low sinuosity in low-relief landscapes, and soft-sediment deformation features and/or mass movement observation in the field (Palmu et al., 2015; Smith et al., 2014). Suspected fault scarps in Fennoscandia, as in other tectonically active regions, have also been confirmed or disproved in the field using paleoseismic trenches (Akçiz et al., 2014; Smith et al., 2014; Mikko et al., 2015; Kozacı et al., 2021). The regional scarp and possible fault dataset and detailed adaptation of scarp classification methods for use in eastern Canada and the northeastern USA (presented by Gourdeau et al., 2023) and the key points relevant to the Saint-Liguori scarp are summarized here.

The Saint-Liguori scarp is situated in a low-relief, semi-agricultural area approximately 50 km north of the city center of Montréal (Fig. 1a) (see Section Data and code availability for links to all field pictures) . Land use in the area is dominated by small-scale grain and vegetable farming and maple syrup production. We mapped glacial features, whose apparent displacement or change in appearance across the scarp helped establish the scarp as a potential fault trace. North-south trending ridges ±1 metre tall are the signature of ice flow, although they have not been associated with any particular advance (Fig. 2a). These ridges are expressed as bedrock grooves south of the scarp and as drumlins in a few places north of the scarp (Fig. 2b). Areas of bedrock exposure or very thin soil cover south of the scarp are unfavorable for farming and the presence of the scarp makes the terrain hard to plow. As a consequence, the scarp often delineates the end of the farmed land and the beginning of the forest cultivated for maple syrup production. We suggest that the distribution of agricultural land use was selected by early farmers for the flat areas underlain by deeper sediment, and subsequent activity likely removed any local relief along the scarp where possible.

The Saint-Liguori scarp, more than any other observed lineament observed within a 100 km-area around the city of Montréal, met the criteria for a feature of interest (Gourdeau et al., 2023). The scarp is expressed as a nearly continuous, >5 km-long, ENE-trending topographic scarp about 2-3.5 metres high, with bedrock exposure consistently appearing on the south side (Fig. 2d, e, 3). Quaternary sedimentary deposits are discontinuous across the scarp (see Fig. 2a). The scarp is higher (2-3 m) in the forest and lower (0.5-1 m) in the plowed fields (Fig. 2a and b). Several shallow channels make sharp local bends at the scarp. The scarp is best preserved where the bedrock is exposed at the surface on the south side (Fig. 2b). The middle section of the scarp displays more complexity, as a km-long discontinuous stepover appears with a secondary strand 100-200 m south of the main strand (Fig. 2b). The topographic scarp tapers in height to its endpoints, which disappear into agricultural fields (black arrows in Fig. 2a). Where the scarp crosses the flood-plains of the Ouareau River, it is locally affected by fluvial terrace modification (Fig. 2b).

4 Field investigations

We walked approximately 90% of the length of the identified scarp with the permission of 14 private landowners (see Acknowledgements). A ∼1 m-deep, test pit was excavated on the northern side of the scarp to examine

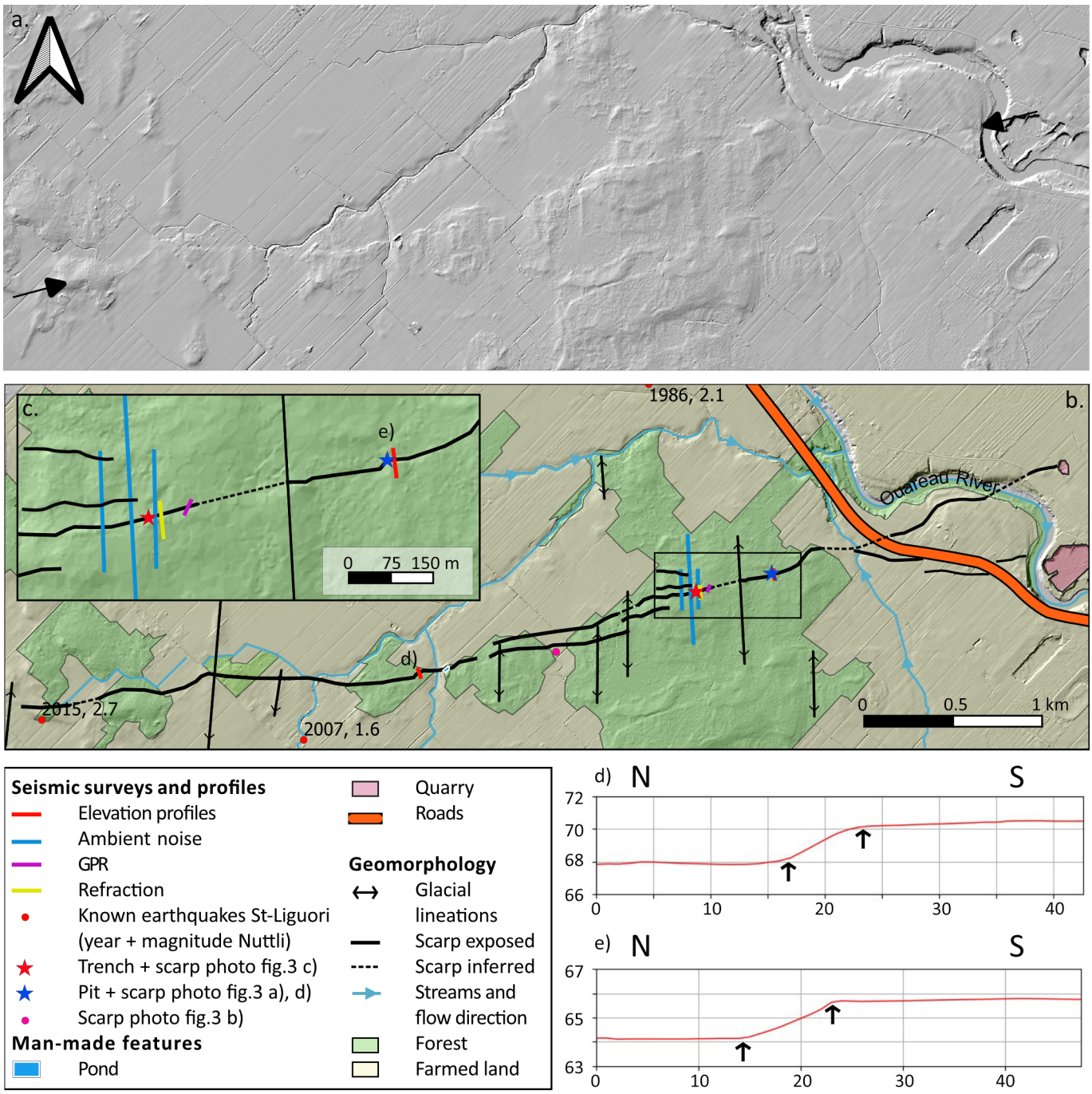

Figure 2 a) Lidar-derived hillshade of the Saint-Liguori scarp (light orientation is 315°, altitude of 45°, Z factor of 2. The scarp is located between the two black arrows. The original hummocky glacial geomorphology is very visible in the forested areas where the landscape hasn't been smoothed by farming. b) Geomorphic map of the study area indicating scarp location, land cover type, and geophysical sampling locations. c) map inset of the trench area showing the location of the three geophysical surveys, the test pit and the trench. d) and e) are elevation profiles crossing the scarp. The location of the profiles are indicated on map b) and inset c), respectively. The black arrows are pointing at the location of the scarp.
En français: Carte ombrée dérivée d'imagerie lidar de l'escarpement de Saint-Liguori (orientation de la lumière 315°,altitude de 45°, facteur Z de 2). L'escarpement se situe entre les flèches noires. La géomorphologie irrégulière originale est visible dans la forêt, là où le territoire n'a pas été aplani par l'agriculture. b) Carte géomorphique de la zone d'étude comprenant la position de l'escarpement, le type de végétation et le positionement des levés géophysiques. c) carte agrandie de la zone où la tranchée a été réalisée comprenant le positionement des 3 levés géophysiques et de l'excavation contrôle. d) et e) représentent des profils topographiques prélevés perpendiculairement à l'escarpement. La position des profils est indiquée sur la carte b) et c), respectivement. Les flèches noires indiquent la position de l'escarpement.

shallow sediments.

The forested areas crossed by the scarp (pale green, hummocky terrane; Fig. 2b) have rough topography associated with the bedrock glacial lineaments on the south side of the scarp (Fig. 2a, b). The forests are young (≤100 years) and are managed for maple syrup produc-

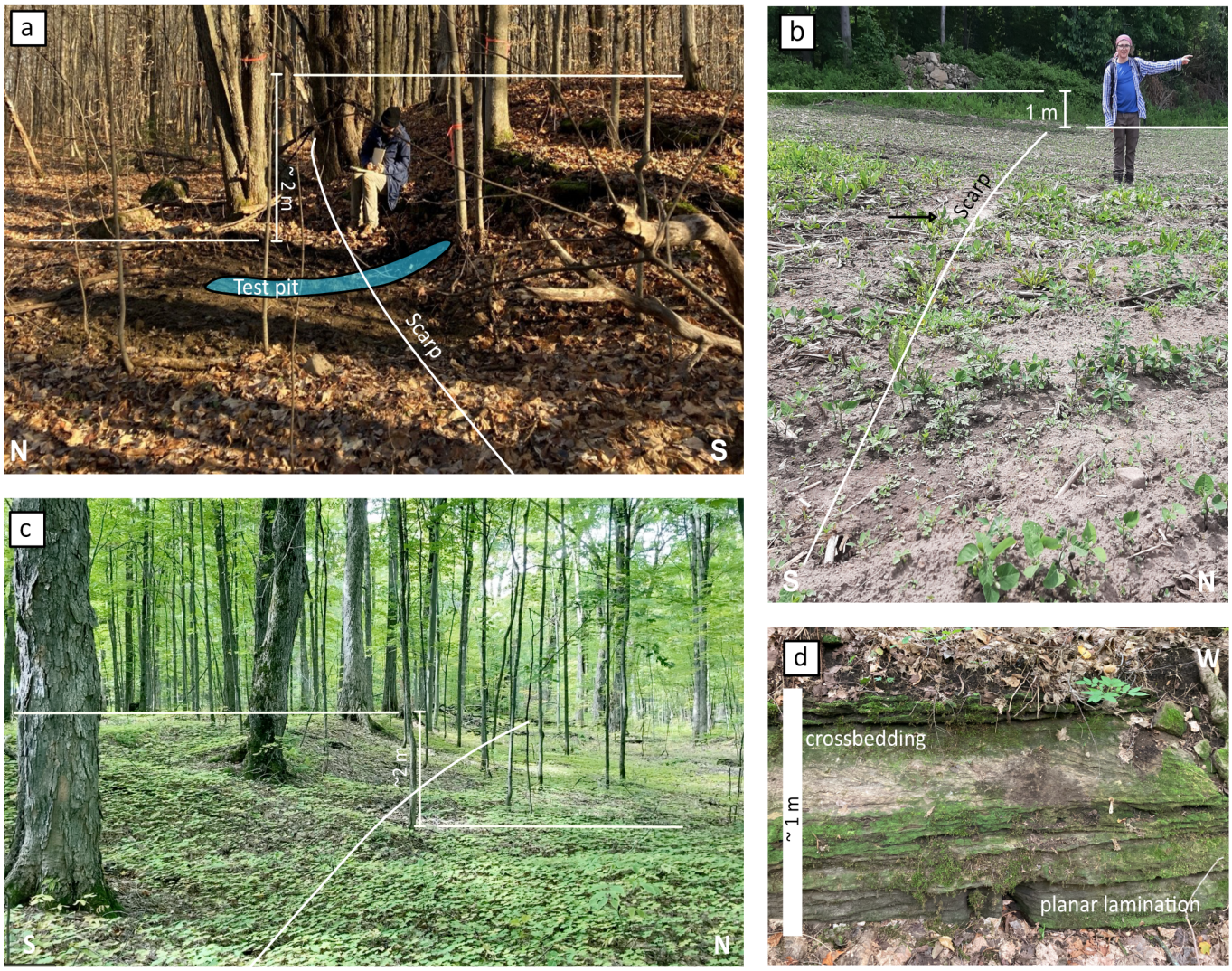

Figure 3 Expression of the scarp in the field. Base of scarp is marked with white lines in a), b), and c). Thin white lines marking approximate local relief. a) Expression of the scarp in the forest, where the test pit was excavated (blue polygon shows extent of pit footprint; see blue star fig. 2 for location). The height is large (2 m), the scarp is sharp, and the bedrock is exposed on the upper surface. b) Expression of the scarp in the farmed area, in the southern branch of the suspected stepover near the center of the mapped scarp length (see pink dot fig. 2 for location). The scarp is subtle, but ∼1 m of relief is still visible. The bedrock is exposed, compromising vegetable growth. c) View looking west along the scarp at the location of the paleoseismic trench, showing continuity and consistency of scarp height (see red star fig. 2 for location). d) Exposed bedrock on the scarp near (a). Planar laminated dolostones at the base are overlain by crossbedded calcite-cemented pebbly quartz sandstone. The top of the scarp displays ∼30 cm soil development (covered with leaves).
En français: Apparence de l'escarpement sur le terrain. La base de l'escarpement est définie par des lignes blanches en a), b) et c). Les autres lignes blanches et fines indiquent la position approximative du relief de l'escarpement. a) Apparence de l'escarpement dans la forêt, là où l'excavation contrôle a été effectuée (le polygone bleu indique l'étendue de l'excavation à la surface) (voir étoile bleue fig. 2 pour connaître le positionnement). La hauteur est importante (2 m), l'escarpement est net et le socle rocheux est exposé en surface. b) Apparence de l'escarpement dans les champs cultivés, sur l'embranchement Sud du possible stepover près du centre de l'escarpement (voir point rose fig. 2 pour connaître le positionnement). L'escarpement y est plus subtil, mais ∼1 m de relief est tout de même visible. Le socle rocheux est exposé dans le champs, rendant la culture de légumes impossible. c) Vue de l'escarpement en direction Ouest, près de la tranchée paléosismique (voir étoile rouge fig. 2 pour connaître le positionnement). La constance et la continuité dans le relief de l'escarpement y sont bien visibles. d) Socle rocheux exposé près de la photo (a). Des dolomies planaires et laminées à la base sont surmontées de grès cimentés par de la calcite et comportent des lits croisés. Le haut de l'escarpement est surmonté par ∼30 cm de sol (couvert de feuilles).

tion. Glacial erratic boulders of plutonic and gneissic rock are scattered on the land surface on both sides of the scarp, and many were observed partially buried where unconsolidated sediments are sufficiently thick.

The bedrock exposed along the scarp is a thin-bedded calcareous pebbly quartz sandstone (Fig. 3d). Finer layers of dolomitic to calcareous laminiated silt-sandstone are more deeply weathered. The erosion of these layers gives a step-like appearance to the bedrock scarp face (Fig. 3d). The 10-30 cm coarse pebbly sand layers are massive or crossbedded. These layers are made of 80% coarse, rounded, spherical, and well-sorted grains

of quartz and feldspar with 5% <0.5 cm bioclasts and white-grey calcite cement.

4.1 Test pit

We excavated a ∼90 cm-deep test pit to investigate the unconsolidated sediments on the north side of the scarp (Figs. 3a). The east wall was cleaned and photographed for construction of a 3D photomosaic using Agisoft Metashape (Fig. 4, Table 1; See Section Data and code availability for links to all repositories.). The soil present at the surface is a homogeneous, organic-rich, sediment-poor dark brown soil 30-35 cm thick, containing abundant roots of 0.5 cm to 4 cm in diameter. Approximately 60% of the soil is made of coarse to medium, moderately well-sorted quartz sand with trace micas. The soil also contains <3% 2-15 cm subangular gravel. Below the active soil layer is dense, light to medium brown compacted sandy loam. The uppermost ∼25 cm is massive, clayey, and contains roots. This layer fines gradationally downward and is predominantly made of silt and clay with 40% medium-coarse sand. Rare cobbles and gravel were observed in the horizon, which also contains small oxidized spots surrounded by iron oxide cement (possible filled burrows). The deepest burrows were observed at 55 cm below the ground surface and have a maximum length of 10 cm.

This horizon is underlain by ∼5-10 cm layers of tan sand with blue-gray lenses. Orange iron oxide cements are abundant in the sand layers. The lenses are ∼1-3 cm thick and give way to more continuous layers at about 70 cm below the ground surface. The layers dip moderately north on the north wall of the pit and steepen to the south as they approach the steep bedrock contact (Fig. 4). Due to the alignment of some coarser sand laminae with the grey clay layers, we tentatively identified the layering as primary. The primary layering is accentuated by concentrations of authigenic iron oxide along parallel but irregular layers. The layers steepen toward the bedrock contact. Bedrock on the south wall of the pit was similar to that observed at the surface, and bedrock was not encountered north of the scarp.

4.2 Ground Penetrating Radar

The Ground Penetrating Radar (GPR) survey was run on the 8th of February 2022, at ambient temperatures of -2°C, while the soil was completely frozen (See Section Data and code availability for links to all repositories.). The GPR used was a PulseEKKO PRO model 1100 with 100 Mhz antennas. The time window was set at 200 ns, the temporal sampling interval at 0.8 ns, the antenna separation at 1 m, and the step size at 0.25 m. Figure 5 is interpreted using radar velocity in the subsurface at 0.165 m/ns, an appropriate velocity for ice. The parameters were set to reach as deep as possible despite the expected loss in resolution. A single 30 m-long line was run from NNE to SSW (purple line on Fig. 2b). We ran that non-perpendicular transect due to heavy vegetation and deep snow surrounding the area (purple line on Fig. 2b). The raw GPR scan (Fig. 5a) shows the presence of significant dipping reflectors at ∼0-10 m, aligned with with the surface expression of the scarp.

The raw data obtained in the field was visualized and processed using the free program Reflex 2D-quick and EKKO project V5. The data was processed by doing a static correction (repositioning the Y-axis to zero), a background removal (removing the average trace to remove surface wave and constant horizontal reflections), applying a standard SEC gain to amplify late reflections, and applying a topographic correction to correct the surface elevation profile using the GPS data. The rest of the parameters were kept at default. The color contrast was maintained to default.

Assuming the frozen soil approximates the radar velocity of ice (Fig. 5), the reflector corresponding to the surface scarp dips gently (20°) NNE down to a depth of ∼2.5-3 m and is overlain by a zone of more chaotic reflectors gently dipping in both the NNE and the SSW direction (blue). We interpreted these chaotic reflectors as poorly stratified or disrupted sediments. These chaotic reflectors could be related to mixed grain sizes in the matrix, changes in soil composition, and/or disorganized and randomly oriented clasts, which we hypothesized could represent disruption in the hanging wall of a normal fault. The bedrock is buried ∼3 m at the NNE end of the line, at the junction of the strong bedrock reflectors contact (orange line, gently sloping down SSW) and the inferred fault (see Fig. 5). These most prominent bedrock reflections (orange line) are visible at ∼5 m depth, with some deeper reflections visible at up to 10 m, and were interpreted to represent bedding planes in the bedrock. Above the bedrock, a weathered, saturated transition zone is interpreted (orange). The red and almost horizontal reflectors in the zone are interpreted to be related to the progressive freezing of the water table due to their nearly horizontal shape and presence only in the weathered and not consolidated bedrock zone. The reflectors overlying the interpreted bedrock-sediment contact (green line) follow the shallow dip of the bedrock-sediments contact (Fig. 5c). They were interpreted to represent unconsolidated stratified sediments. The bedrock-sediment contact is the shallowest at 10 m along the line, concurrent with the surface expression of the scarp. The GPR profile interpretation was consistent with the precedent observations, leading us to pursue our investgations.

4.3 Ambient noise recordings

To estimate the depth to bedrock over a wider area, a campaign of ambient noise recording was carried out at 21 sites on Oct. 27th, 2022 (See Section Data and code availability for links to all repositories). The sites were selected along three lines perpendicular to the scarp, close to the GPR survey line. Ambient noise was recorded for 20 minutes on each site using Tromino© sensors setup in a flat zone. The records were analyzed using the Horizontal-to-Vertical Spectral Ratio (HVSR) method to estimate the fundamental resonance frequency (f_0) on site (refer to Molnar et al., 2018, for more details). The data were analyzed with the Geopsy software (Wathelet et al., 2020) and following the standard procedure described in the SESAME project (Ac-

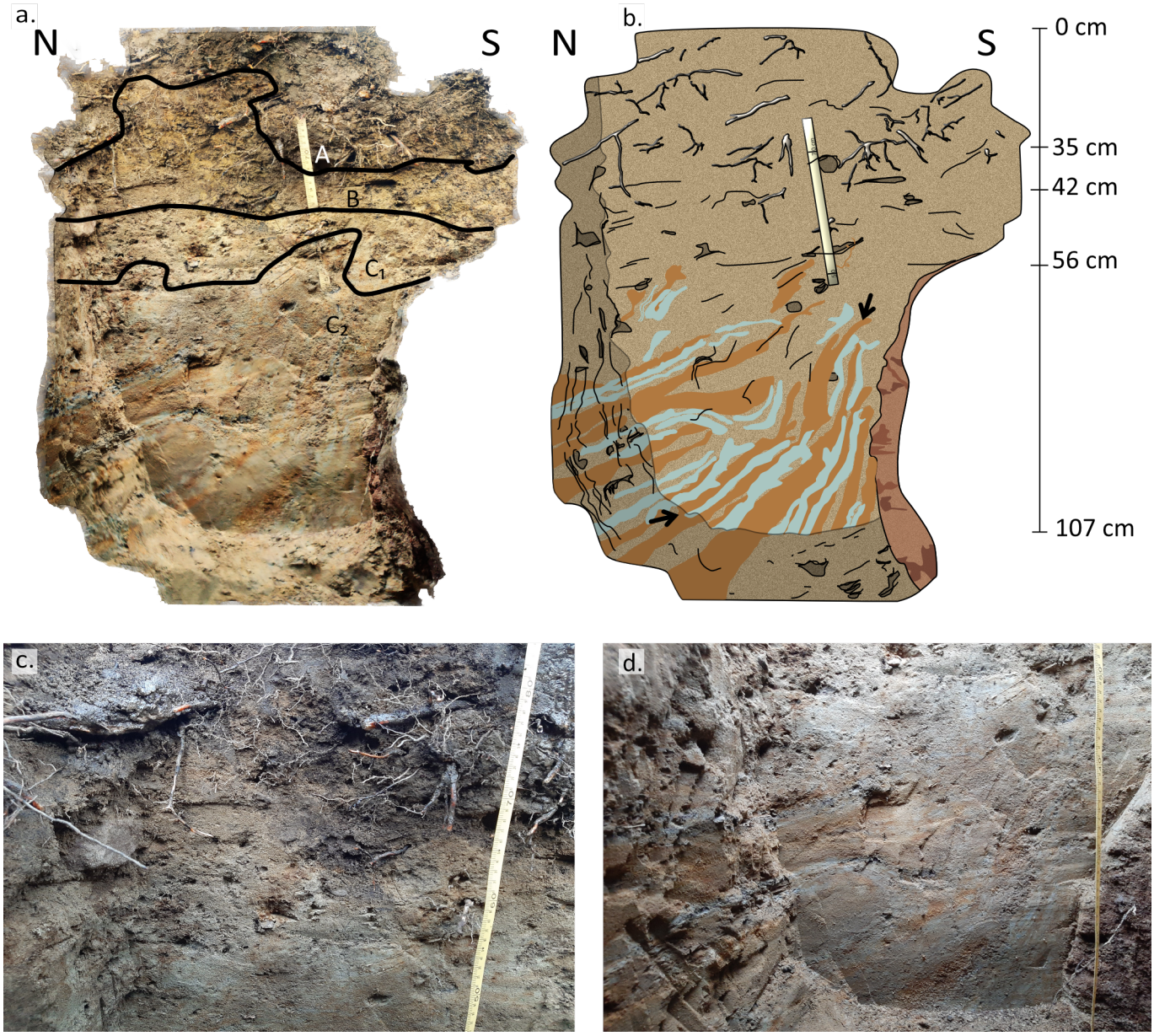

Figure 4 a) Eastern wall of the test pit from Agisoft Metashape model. Tape measure for scale. b) Sketch of (a), emphasizing key features. The bedrock is in reddish-brown on the southern wall of the pit. At the bottom (∼56-107 cm below ground surface), blue and orange clay beds display steepening toward the bedrock interface (black arrows). This is overlain by homogeneous sandy loam 35-56 cm). The surface is organic and root-rich soil (0-35 cm). Scale in yellow. The labels A, B, C1, and C2 represent the soil horizons presented in table 1 c) Close-up of the upper organic-rich soil horizon. d) Close-up of the basal clay beds observed at the bottom of the pit.
En français: Mur est de l'excavation contrôle obtenu grâce à un modèle Agisoft Metashape. Ruban à mesurer pour l'échelle. b) Croquis de (a) soulignant les éléments clés de l'exacavation. Le socle rocheux est rougeâtre le long du mur Sud. Le bas de la colonne (56-107 cm) comporte des lits d'argile bleus et oranges courbés, pointés entre les deux flèches noires. Les lits sont de plus en plus verticaux près du socle rocheux. Cette partie est surmontée par 35 à 56 cm de limon sableux homogène. La partie de 0-35 cm est riche en racines et en matière organique. L'échelle est identifiée en jaune. Les étiquettes A, B, C1 et C2 représentent les horizons décrits dans le tableau 1. c) Agrandissement de la partie riche en matière organique du haut de la colonne. d) Agrandissement des lits argileux observés au bas de l'excavation.

erra et al., 2004). The map in Figure 6 locates the investigated sites grouped by predominant frequency of the peak amplitude f_0 as estimated in the HVSR spectrum. The entirety of the spectra for the 21 sites can be found in the supplementary materials (See Section Data and code availability for links to all repositories).

The survey results indicate the presence of a thicker layer of sediments north of the scarp where the values of f_0 are lowest (around 10-12 Hz) and very shallow bedrock south of the scarp (with higher values of f_0), consistent with the GPR results. The value of f_0 is related to the layer thickness (H) and average shear-wave velocity (Vs) such that f_0 = Vs/4H (Roesset, 1970), assuming a homogeneous soft surface layer with a Vs of 200 m/s (as suggested by Rosset et al., 2015). The thickest sediments (∼4 m to bedrock) appear at sites B5, B6,

Depth (cm)	Label	Description	Color
Surface (0-4)	O	Uneven surface covered in maple leaves and organic material	
4-35	A	Organic-rich, many roots. Contact irregular, possibly due to tree uprooting and tilling. Contains sub-angular gravel.	Gray-brown
35-42	B	35-42 B Reduction in roots, increase in sand. Noticeably more yellow color.	Yellow-brown
42-56	C_1	Sandy parent material (40% medium-coarse sand, 60% silt and clays), fining gradationally downwards. Rare cobbles. Oxidized layers, possibly reflecting water flow paths.	Tan
56-107	C_2	Tan sand with blue-gray lenses. Abundant orange iron oxide layers.	Tan sand, blue-gray clay-rich layers

Table 1 Description of soil units in the test pit

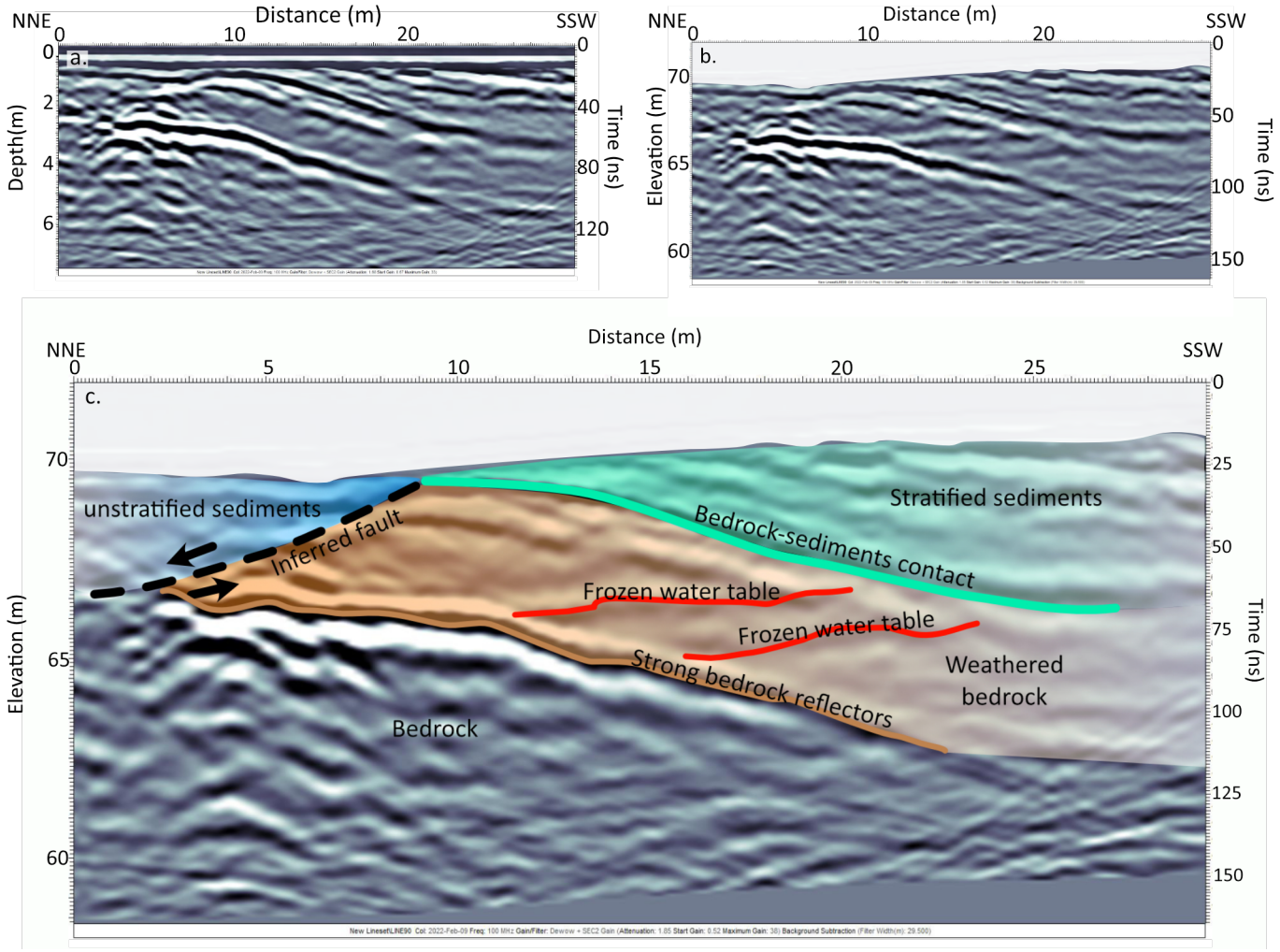

Figure 5 a) The raw data obtained from the GPR survey using EKKO project V5, b) GPR survey after processing, with topography considered, using EKKO project V5. Vertical axis is depth assuming uniform velocity of ice. c) Interpretation of the processed GPR survey. Calculated depths(m) are assuming a velocity of ice (v = 165 m/ns).
En français: a) Données brutes des levés GPR obtenues à l'aide de EKKO project V5. b) Levé GPR après avoir traité les données à l'aide de EKKO project V5. L'axe des ordonnées représente la profondeur selon la vitesse dans la glace. c) Interprétation des données GPR traitées. Les profondeurs calculées utilisent la vitesse de la glace (v = 165[m/ns]).

B7, and C2, a couple of metres north of the scarp. Frequencies at sites B1 and B2 further north suggest similar thicknesses while the sites A1, B3, B4, and C1 suggest very shallow bedrock. The uncertainty associated with the depth estimate is significant, but this does not detract from the distribution of frequency values over the area, which indicates a relatively thicker layer of unconsoildated sediment north of the scarp.

4.4 Seismic refraction survey

A seismic refraction survey was run perpendicular to the scarp in the same location as the ambient noise survey (Fig. 2, See Section Data and code availability for links to all repositories). Twenty-four geophones were spaced at a 2 m intervals along the survey line and three source shots were hammered per array location (at -2 m, 23 m, 48 m respectively). Each geophone was moved 2 m northward to shift the array after each set of three

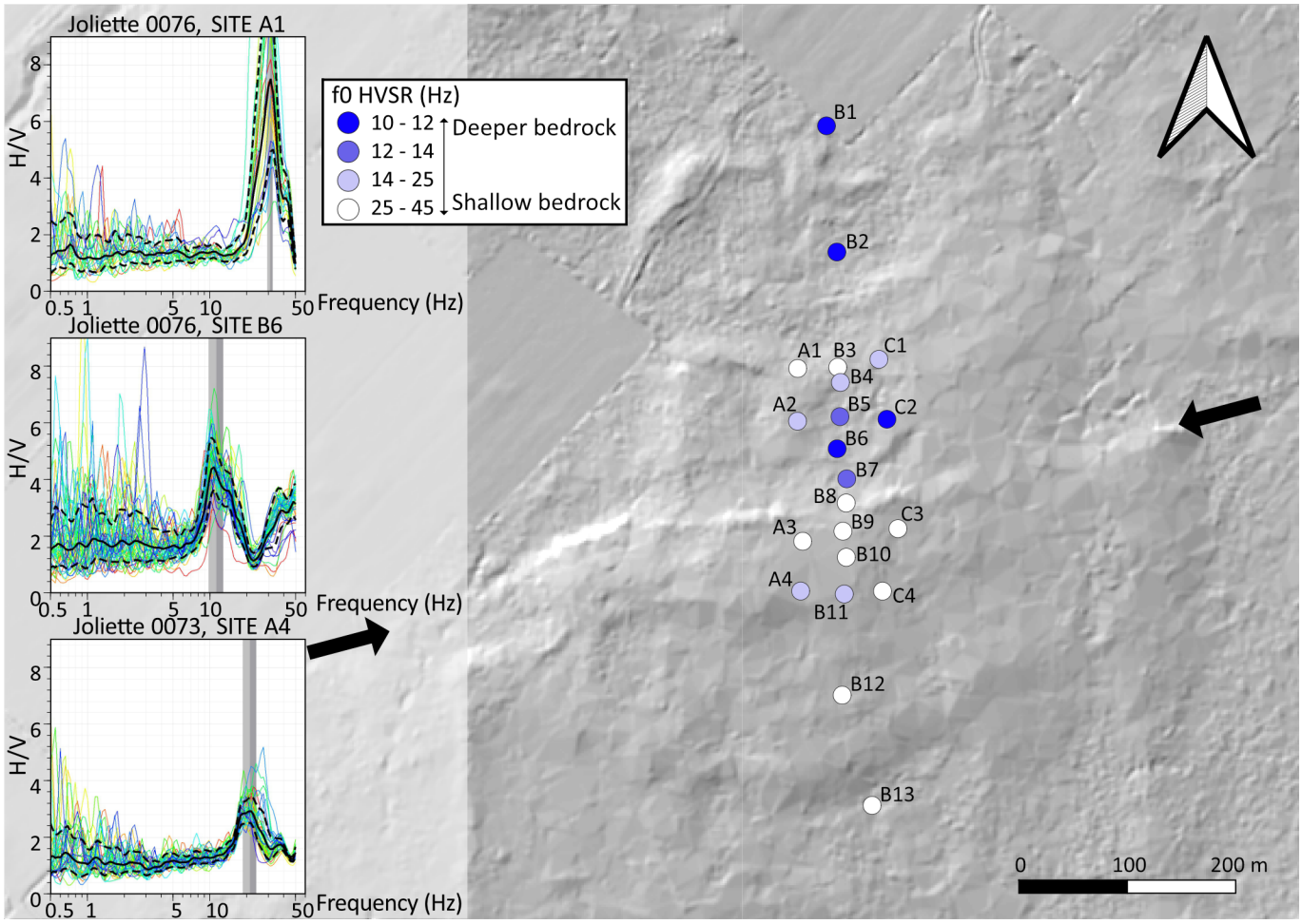

Figure 6 Ambient noise recording locations superimposed on lidar DEM (see Fig. 2 for location). The scarp appears between the black arrows. Three ambient noise profiles (A, B, and C) were collected perpendicular to the scarp. The point's colors indicate the predominant frequency sampled at each site, which is roughly correlated to the bedrock depth at these locations. Three ambient noise HVSR spectra are presented on the left side of the plot for reference. The spectra for the 21 sites can be found in the supplementary materials (Section 7).

En français: Localisation des enregistrements de bruit sismique et carte lidar ombrée (voir Fig. 2 pour positionnement). Les deux flèches noires localisent l'escarpement. Les enregistrements de bruit sismique sont localisés selon trois profils (A, B et C) perpendiculaire à l'escarpement. La couleur des ronds indique la fréquence prédominante f0 calculée pour chaque site, qui est inversement proportionnelle à la profondeur du socle rocheux. Trois exemples de spectres HVSR de bruit sismique sont présentés du côté gauche de la figure. Les spectres HVSR obtenus pour les 21 sites sont accessibles dans les documents complémentaires (Section 7).

shots, resulting in a total effective survey length of 64 m. The data was filtered between 100 and 300 Hz and grouped into common shot gathers. First arrivals were picked manually using Refrapy (Guedes et al., 2022). The picked travel times were inverted for Vp to derive a 2D model using pygimli (Rücker et al., 2017). The 2D model included the local elevation profile along the seismic line. The starting model for inversion extended to 16 m depth, and the initial velocity structure was a linear gradient from 300 m/s at the top of the model to 3000 m/s at the bottom. The model used an unstructured triangular mesh designed to provide the highest spatial resolution in areas with the most data coverage. The final velocity model is the result of iterative inversion, stopping when the change in the data objective function between iterations is less than 0.1%. The inversion is constrained to keep all velocities between a minimum of 100 m/s and a maximum of 4500 m/s. Figure 7 shows the final Vp model for the region where the data provide constraints.

The resolution of the model was assessed using superimposed checkerboard velocity anomalies (Zelt, 1998). The data can resolve velocity structure in a smooth sense but, due to sparse ray coverage, the nominal resolution limit for the model is ~8 m, meaning that velocity anomalies with a smaller length scale than 8 m may not be faithfully resolved in most of the model space. Thus, the refraction survey is broadly consistent with the results of the other geophysical investigations, but does not add any additional constraints on the subsurface structure.

5 Saint-Liguori trench

The geophysical and test pit observations presented above seemed to be consistent with the hypothesis that

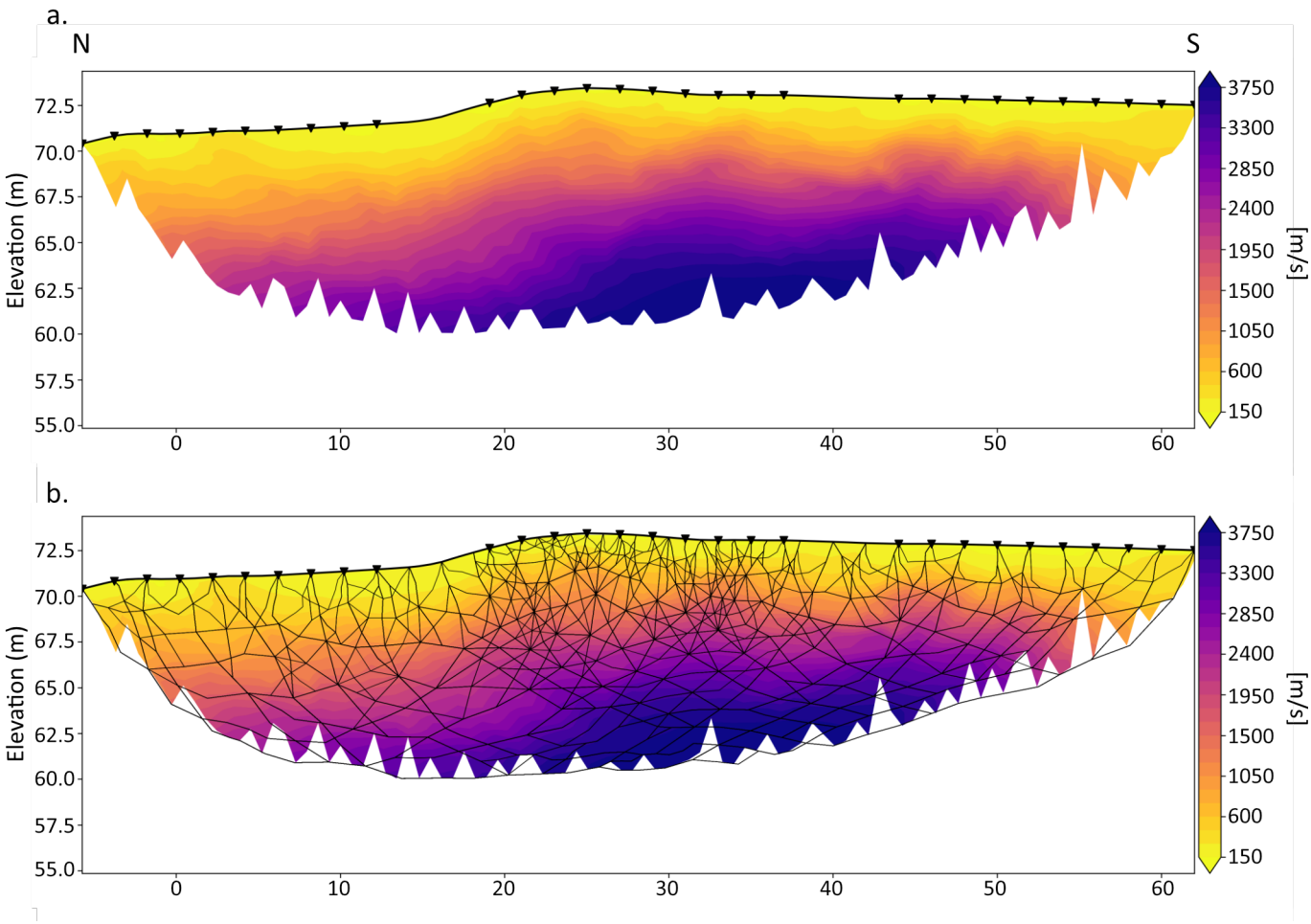

Figure 7 a) Processed and smoothed refraction survey results. b) Refraction velocity model with ray coverage.
En français: a) Profil de sismique réfraction après lissage b) Profil incluant la couverture des rais sismiques.

the Saint-Liguori scarp could be a post-glacial fault scarp, motivating us to excavate a paleoseismic trench at Cabane à Papio near the village of Saint-Liguori in summer 2023 (Fig. 1, 8). The trench site was chosen in consultation with the landowner, where the highest part of the scarp was accessible by four-wheeler tracks and the population of large producing maple trees was least dense. Québec law (s. 3.15.3.1(1),(2),and (3) of the Code de sécurité pour les travaux de construction) requires oversight by a professional engineer for excavations greater than 1.2 metres deep (Gouvernement du Québec, 1979). Under the law, generic excavations must be fully shored prior to allowing people working within walls >1.2 m high except in cases of certification by a professionally accredited engineer. An initial consultation with an engineering company resulted in a shoring design that could be slid along the trench wall to reveal 20 cm-square windows of the soil. We rejected this plan as untenable because it would not allow for cleaning and photographing the walls. We also contacted several government agencies and found that those with a geological mapping mandate had no experience with trenching and those overseeing roadworks had no experience with soil logging at the level of detail required for a paleoseismic trench investigation. No agency was able to offer advice or support on how to legally excavate. For several months it appeared there was no legal path forward to excavating a paleoseismic trench for logging at the site.

The breakthrough occurred through the introduction of a geotechnical engineer who had gained previous experience in paleoseismic studies (Claudine Nackers, P.Eng., M.A.Sc.). She designed a site-specific safety and excavation plan to allow trench wall cleaning and observation with contingencies depending on stability conditions encountered in the subsurface. This plan is compliant with requirements under Québec law, and engineering oversight during the excavation ensured that all conditions encountered were safe. Isra Excavation, a local company, worked closely with the engineer to ensure compliance with safety mandates and to plan adaptations after an intense rainstorm arrived while the trench was open. The benching geometry was agreed upon between the engineer and the excavator operator as the excavation continued. The site safety plan (in French) is available in the supplementary material(Section Data and code availability).

The trench was opened on 13 July 2023 and reached a depth of 3.15 m (of which only 2.93 m was logged for safety reasons) by 9.12 m long and 4.2 m wide at the surface, with four benches on each long side. The south wall of the trench was bounded by the bedrock scarp, which was cleared of soil to the top of the topographic scarp. Slabs of detached bedrock up to 1 metre

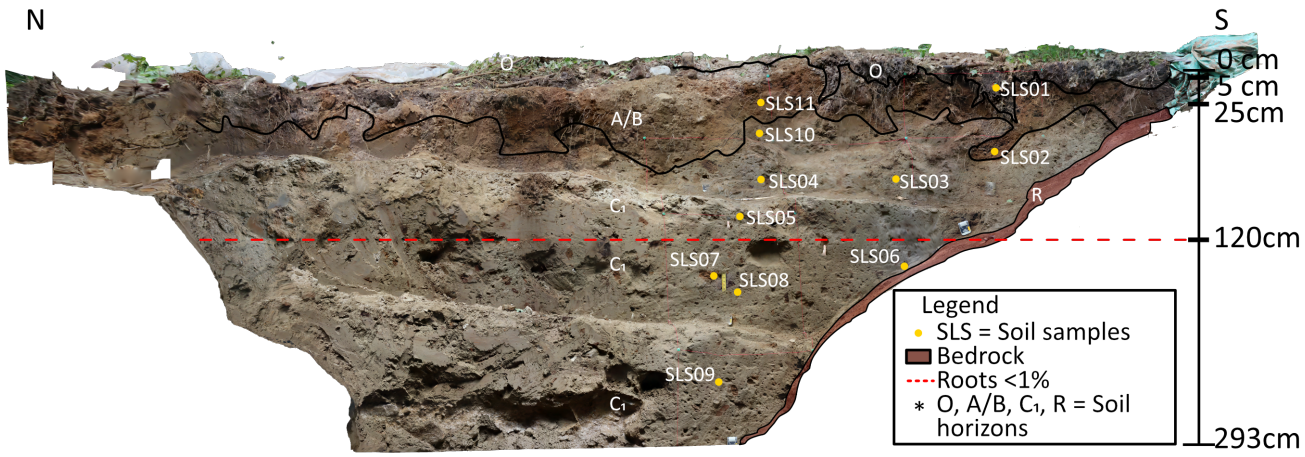

Figure 8 Agisoft orthophoto of the eastern wall of the trench. The soil sample locations shown with yellow dots were used for Munsell color identification and collected for grain size analysis but not yet analyzed. The horizon names and positions are also included in the orthophoto. The sharp contacts bounding horizons O and A, marked with black lines.
En français: Orthophoto du mur est de la tranchée obtenue à l'aide d'Agisoft. Les échantillons de sol prélevés sur le mur sont identifiés en jaune. Ils ont été échantillonnés afin de déterminer la couleur des horizons à l'aide d'une charte des couleurs des sols de Munsell et pour une potentielle analyse de la granulométrie. Le nom des horizons et leur postion sont aussi inclus dans l'orthophoto. Les horizons O et A, qui sont délimités par des limites nettes, sont identifiés à l'aide de lignes noires.

wide were removed from the trench by the excavator, but no similar slabs were observed as clasts in the sediment. The dense diamict matrix (described below) was slightly moist and exhibited high cohesion, resulting in favorable conditions for wall cleaning and photography (See Section Data and code availability for links to all repositories). The north wall of the trench was not cleaned. The east and west walls were benched (Fig. 8) at intervals of 0.75-1.2 m to a width of 0.5 metres, with benches sloping gently toward the south. The east wall was cleaned for photography and logging. The west wall was partially cleaned in the area adjacent to the bedrock scarp. The 3D model is available in the supplementary materials (Section Data and code availability).

5.1 Bedrock description

The bedrock below the ground surface was shaped by bedding plane ledges forming a stepped wall oriented at 340/17W, consistent with the interpreted bedding planes on the GPR. The bedrock comprises interbedded crystalline carbonate, calcite-cemented cross-bedded quartz grits, and reddish fissile siltstone which was not previously identified at the surface scarp. Crystalline carbonate beds (dolostone with some calcite clasts and cement) are golden brown on smooth weathered surfaces and medium gray on fresh surfaces. Lacy siliceous cements decorate wavy – likely algal – laminated beds to about 0.6-1.2 m thick. Benches on the exposed bedrock scarp are topped by thinner (30-40 cm) crossbedded quartz sandstone (0.5-2 mm) beds, with high grain sphericity and rounding. The sand is calcite cemented, resulting in a friable weathered zone extending ~5 cm below the soil interface. Thin (2-5 cm) shale interbeds occur above quartz sandstone beds and sometimes between thicker crystalline carbonate beds. The shales are massive to laminated, dark grey, plastic, and fissile where weathered. Parting surfaces are altered to brick red within a few cm of soil interface.

The bottom of the trench was reached at a subhorizontal bedding plane surface of crystalline carbonate at 293 cm below the ground surface. A deeper bench was reached on the northeast side of the trench, but due to stability concerns related to storm water ponding, we did not log that area below 293 cm. We estimate that the depth reached ~315 cm. Bedding plane slabs of bedrock detached during excavation, aided by joints oriented ~058/90, parallel to the scarp. The steps in the outcrop are formed by the upper surface of carbonate bedding planes, and the base of the ledges corresponds to the erosion of the thin reddish siltstones. This description is consistent with the Beekmantown Group, possibly the Beauharnois Formation (Hersi et al., 2003), as indicated on the regional bedrock geologic map (Ministère des Ressources naturelles et des Forêts, 2021).

5.2 Sediment description

The diamict depositionally overlies the stepped bedrock surface (Figure 8). The contact was observed from the base of the organic-rich soil horizon down to the base of the pit, which was terminated at a wide bench in the bedrock 3 m below ground surface (Table 2; Figure 8).

The excavator removed 30-50 cm of organic-rich, dark brown to chestnut brown soils with abundant (10%) roots 0.5-4 cm in diameter. The soil transitions to unconsolidated but densely compacted matrix-supported diamict. The transition between the upper soils and the diamict appears at a depth of ~25 cm. The contact is sharp, but undulating. Living roots were observed down to 1.2 m below ground surface (<1% roots), penetrating the diamict. A couple of roots reached a depth of 1.5 m, only appearing in highly weathered clasts. The diamict matrix is massive and lacks visible bedding planes, lamination, or grading. Only very subtle changes in grain size, color, and composition were ob-

served from the base of the soil to the bottom of the trench (~2 m). The matrix is pale brown (olive brown 2.5Y 4/2 and 4/3 to olive gray 5Y 4/2), and comprises ~10% clay, 70% silt, and 20% sand.

We observed irregular elongated bodies of nearly 100% brown homogeneous clay in the upper ~0.5-0.75 m of the trench wall. These comprise <1% of the diamict. They are locally branching and irregularly taper and are found in both horizontal and steep orientations, with the horizontal ones up to a few cm in diameter and steep ones more likely to be millimetric in diameter. These appear to follow root traces, and we interpret these as the weathering products of the diamict due to reactions with organic acid from the roots.

5.3 Clast description

In the diamict, the clast size is heterogeneous, varying from <1-20 cm, with rare clasts reaching 30 cm. The clasts had no grain-to-grain contacts and no preferred orientation and were distributed homogeneously in the diamict. They were usually angular and highly weathered. The different clast types observed are summarized in Table 3. We noted three colors of deeply weathered, friable, oxidized clasts (orange, dark brown, and black) that have similar grain textures, suggesting the protolith microstructure was common to all three.

The deeply weathered condition of the clasts across a range of compositions is consistent with the older glacial diamicts known from southern Québec. If correlative, this diamict may be as Illinoian (130-191 ka Shilts, 1992). All the clasts observed in the matrix were plutonic or metamorphic, suggesting that they were not representative of the local geology. No local Paleozoic clasts were identified.

6 Discussion

Based on the geomorphic features of the scarp and the subsurface continuity implied by the geophysical investigations, we interpreted the Saint-Liguori feature as a likely candidate for a recent fault scarp. The bends in drainages flowing southward toward the scarp face (Fig. 2) were identified as possible deflected channels. In retrospect, the deflection does not necessarily represent channel displacement or scarp development, and we cannot be sure how much anthropogenic modification of the channels has taken place. The test pit also strongly suggested that the scarp could have been fault-related. The displacement of Holocene sediments inferred from the geomorphology, combined with the observation of curvature of layers we had interpreted as sedimentary layering against the scarp surface were perceived as drag folds indicating evidence of faulting (Grasemann et al., 2005; Smith et al., 2014; Mikko et al., 2015; Palmu et al., 2015). The data subsequently obtained in the field during the three geophysical surveys consistently indicated a buried bedrock scarp, consistent with a fault offset. These observations, made with multiple techniques, increased our confidence in having found a north side-down normal fault 50 km NNE of Montréal, and near enough to the city to represent the source fault for 1732 ~M5.8 earthquake. Surface rupture is rare for earthquakes <M5-5.5 (Wells and Coppersmith, 1993; Leonard, 2014) and when it occurs, even more rarely produces a scarp under ~5 km long (Biasi and Weldon, 2006). However, noting recent landscape modifications, our mapped scarp length represents a minimum bound for the original feature. If formed by many events, perhaps migrating in space, a preserved scarp may be longer than expected for a single rupture. So the short mapped length of our scarp was not necessarily indicative of its potential to be a paleoseismic feature.

Trenching in July 2023 confirmed the existence of a steep and ~horizontally bedded buried bedrock scarp at least ~3 m deep, but it was found to be depositionally overlain by an old and completely undeformed diamict. The lack of bedding in the diamict corresponds to the chaotic unit overlaying the bedrock interpreted from the GPR profile, and the observed bedding also approximately matches the interpretations made on the GPR (Fig. 5). The diamict displays evidence of intense post-depositional weathering without physical deformation, as evidenced by the preservation of sharp clast boundaries for lithoclasts that are completely friable and weathered beyond identification. If any post-depositional deformation had affected the diamict, we would expect to see disruption of the boundaries, deformation, and disaggregation of these clasts, but they were observed completely intact. The massive matrix of the diamict is homogeneous mixed fine sand-silt with no detectable deformation bands, fractures, fissures, rotated/oriented clasts, or other features typically associated with faulting or shearing in unconsolidated to weakly consolidated sediments (Table 2; c.f. Bray et al., 1994; Oettle and Bray, 2013; Balsamo et al., 2014). Delicate diagenetic/weathering features were observed intact, including the wavy-tabular and tubular clay bodies associated with roots. The roots that formed the clay bodies are older than the modern root systems, so the fact that we do not observe offset or contortion of these features adds to the evidence that the diamict has not experienced deformation. The variable clast lithology is consistent with glacially transported coarse clasts primarily derived from the Grenville belt (granite and quartzite). The deeply weathered orange, brown, and black clasts are of unknown affinity, but based on the color, the protolith may be mafic or ultramafic. Due to the lack of clast alignment and matrix shear fabric and absence of faceted clasts, lack of sorted or laminated beds, the origin of this diamict remains uncertain but the variety and size distribution of lithoclasts, and high matrix fraction, could suggest basal deposition by lodgment or melt-out, melt-out, or debris flow origins in a pro- to subglacial setting.

This study highlights the importance of trenching to accurately identify fault scarps for paleoseismic studies. Although the geophysics results were suggestive, no conclusions could be drawn until the absence of deformation of the sediments was directly observed (c.f. Akçiz et al., 2014). Trenches have been used to assess the seismic origin of scarps and assess the timing of fault activity, notably in related recently deglaciated

Depth (cm)	Soil Horizon	Description	Color
Surface		Uneven surface covered in maple leaves and organic detritus	Variable
0-5, variable	O	Humic. Very abundant roots (15%), cohesive, organic-rich material.	Very dark brown (7.5YR 2.5/1)
5-25, variable	A/B	Sparse fine to medium sand. Lithic sub-angular sand with yellowish quartz. Roots ∼10%. Rare gravel <5%. Contains pebbles and cobbles (similar to the rest of the column). Friable, high porosity. Upper and basal contacts highly convoluted, likely due to tree felling and agricultural disturbance.	Dark yellowish brown (10YR 3/6)
25-293	C_1	Diamict. Near the upper 0.5 m there are wiggly sharp-walled tabular clay bodies, brick brown in color. Most of the thicker (up to 2 cm) clay bodies are sub-horizontal and fine roots emerge from them. Steeper clay bodies ones are more braided, thin (3 mm), and wavy. Matrix is silt to fine sand with 20% medium to coarse sand. <2-5% gravel and around 1% cobbles. <1% boulders. – Subtle transition at ∼120 cm: Abrupt loss of pervasive roots (5% to <1%) and clay bodies. Roots below this level are concentrated in weathered clasts. Subtle color change. Roots are completely absent in the diamict below ∼150 cm.	Olive brown (2.5Y 4/3) At ∼120 cm: subtle color change to Olive brown (2.5Y 4/2) and olive gray (5Y 4/2)
293 – ∼315	C_2	Diamict. Not visible in the photomosaic due to reduced photo coverage at base of pit. Matrix slightly coarser than above (∼ 5-10% increase in the fine to medium sand). Gravel % appears to decrease (around 2%), but overall size increased (2-4 mm predominant). Cobbles <1%.	Olive brown (2.5Y 4/3)
> 293-315 (TD)	R	Bedrock dolostone. depositional contact with diamict to surface at southern pit edge	

Table 2 Description of unconsolidated sediments and soils observed in the Saint-Liguori scarp trench.

Label	Approximate relative clast proportion	Size (cm)	Color	Description
Orange clasts	35%	[0.5-15]	Pale orange	Silt-sized grains, mineralogy uncertain. Homogeneous, & very friable.
Dark brown clasts	33%	[0.5-30]	Dark brown-red	Silt-sized grains with some clay, no zoning, homogeneous. Friable to the point of complete loss of cohesion, angular. Less than 1% gray lithics <0.1 cm.
Quartzite clasts	15%	[1-5]	Bright white	Sugary and friable, angular clasts, almost purely made of quartz. Wide variety of intraclast grain sizes (0.1 cm-1 cm) but homogeneously distributed. Larger grain fraction are sub-angular and represent 10% of the matrix, while tiny grains (<0.5 cm, 90% of the matrix) are rounded. Sometimes present with thin, cohesive dark gray weathered cortices.
Granite clasts	8%	[0.5-7]	Pink	Granite containing coarse 50% k-feldspar, 20% coarse plagioclase, 20% coarse Quartz, and 10% micas of 0.1-0.5 cm. The clasts are sub-angular, hard, and weakly weathered.
Gray greenstone clasts	5%	[1-15]	Gray	Fine-grained, hard, sub-angular pebbles and cobbles. Silicified greenstone. Rough weathered surface with thin cortex.
Black clasts	2%	up to 20	Black	Powdery, highly weathered, and angular clasts. Mineralogy uncertain. May be a darker version of the dark-brown clasts.
Other metamorphic rocks	2%	[0.5-7]	Black and white	Mica-dominated (mica concentration >90%, 0.1-0.3 cm) granites are observed in the matrix. Some gneissic tonalites have also been found in the matrix. Pieces of meta-quartz veins are also observed.

Table 3 Diamict clast descriptions from trench wall.

and intraplate landscapes, and have proved their worth (Markovaara-Koivisto et al., 2020; Figueiredo et al., 2022; Mörner et al., 2000). Even in active plate boundary settings, with strong geomorphic expression of fast-slipping faults with recent ruptures, not every paleoseismic trench is successful (Akçiz et al., 2014).

Although we did not discover a recently active fault, this project still has an important value, since it represents the first paleoseismic trench attempted in Québec. One of the strong outcomes of this project was the creation of a network of engineers, geologists, and governmental agencies that are now familiar with the field of paleoseismology and the protocols associated with paleoseismic work. Together, the techniques used in this paper and the trench establish a set of guidelines that will simplify the study of other scarps in Québec and stimulate the emergence of paleoseismic studies. As suggested by Brooks and Adams (2020), the availabil-

ity of new landscape data such as lidar-derived elevation models should facilitate the discovery of new candidates of glacially-induced or younger faults in eastern Canada. Once surface-rupturing scarps will be found, age estimates could be established by dating fault gouges using 40Ar/39Ar (Vrolijk et al., 2018) or OSL dating (Hu et al., 2024). Precise magnitude estimates and potential recurrence could also be estimated from these scarps using Quaternary geomorphic features, which are abundant in the province, and their measured offset (Morell et al., 2020). Other techniques to estimate the position and magnitude of past earthquakes also remain to be tested in Québec. Notably, the study of precariously balanced rocks (PBRs) sitting on bedrock can reveal a constraint on the time elapsed since the region experienced ground acceleration sufficient to topple the boulder (Weichert, 1994; Brune, 1996). This technique has already been used in Central California and Eastern U.S, but has yet to be tested in Eastern Canada (Rood et al., 2020). These observations will open the way for fault source models, earthquake source models and probabilistic seismic hazard analysis (PSHA) (Morell et al., 2020). Without the discovery of fault scarps, it is not possible to constrain source-specific seismic hazard scenarios, in particular for eastern Canada's major cities (Rosset et al., 2021, 2023).

7 Conclusion

A wide range of techniques have been used to assess the nature of the Saint-Liguori scarp. The lidar-derived data product, the test pit, and the three geophysical surveys all revealed details consistent with disrupted sediments or offset bedrock that led to a consistent conclusion: this scarp was likely to be a fault scarp. However, opening a paleoseismic trench in July 2023 revealed the absence of syn- or post-glacial deformation in a very old diamict buried against the bedrock scarp, completely disproving our earlier interpretation. The scarp is not a surface-rupturing post-glacial fault scarp. This unexpected finding highlights the importance of paleoseismic trenches for identifying active faults. Challenging environments, such as the heavily vegetated and recently deglaciated landscape of southern Québec make fault identification challenging, particularly in light of the low regional strain rate. This paper documents an important breakthrough in the field of intracratonic paleoseismology in eastern Canada, since it represents the first paleoseismic trench attempted in the province of Québec. This project facilitated the development the creation of a network of geoscientists and engineers who are now aware of and interested in intraplate trenching and paleoseismology. This network will be crucial in the upcoming years, since governmental policies and laws in Québec do not account for the logistical demands of paleoseismology, creating a barrier to fault mapping and the development of a prehistoric seismic record for the region.

Acknowledgements

Remerciements: Nous aimerions remercier tous les propriétaires nous ayant permis d'effectuer des recherches sur leur terrain, incluant André, Anthony, François, Jacques, Johanne, Marc, Mathieu, Mr. Gagnon, Philippe Desjardins, Sylvain et sa femme, ainsi que Yves. Merci aussi à Richard qui nous a laissées effectuer des levés sismiques sur sa propriété.

Un merci particulier à Mario Richer et sa fille, et Jannot qui nous ont permis de creuser une tranchée paléosismique au sein de leur ferme acéricole au nom de la science, et qui étaient toujours prêts à nous aider à l'aide de leurs VTTs et de leurs bonnes blagues. Finalement, merci à Israël/Isra Excavation qui a creusé la tranchée avec précaution et minutie.

Acknowledgements: We thank Félix Gervais at Montréal Polytechnique for introducing the geologists to the engineer which enabled this project to move forward.

Thanks to Kaiyuan Wang, Lan Xi Zhu, and Justin Chien for untying the knots during the refraction survey. Thanks to Maximilien Laly for helping with QGIS and ArcGIS. Thanks to Adil Takahashi for the help with the ambient noise survey. Merci à Miguel Saint-Denis pour avoir exploré l'escarpement avec nous. Thank you to Suzanne Owen at McGill Risk Management for making sure that everything we planned was legal. Thank you to Fiona Darbyshire for lending the Ground Penetrating Radar and to Yajing Liu for lending the geophones. Thanks to Bruce Harrison and Kyle Gallant at the New Mexico Institute of Mining and Technology who gave us very good feedback regarding the soil samples and descriptions.

We would also like to thank our reviewers, John Adams and Jack Williams, who provided very helpful and actionable comments that improved the overall quality of the paper.

The EKKO Project license was provided by the EarthScope Consortium through the PASSCAL Instrument Center at New Mexico Tech. The facilities of EarthScope Consortium are supported by the National Science Foundation's Seismological Facility for the Advancement of Geoscience (SAGE) Award under Cooperative Support Agreement EAR-1851048.

Funding was provided by the National Science and Engineering Research Council, Canada (Discovery grant and Canada Research Chairs awards to Christie Rowe) and a Wares Faculty Scholarship to Rowe which supported Prush's postdoctoral fellowship. Aube Gourdeau was supported by a scholarship from Geotop (FRQNT), Helgi Soutar Masters Fellowship and the Eric Mountjoy Fellowship from McGill University.

Data and code availability

Data associated with this project will be publicly available at Borealis.ca. The data files include: Complete Agisoft Metashape model of the trench wall, including component photo set and a 3D model of the trench (https://doi.org/10.5683/SP3/7OZT0V), a complete Agisoft Metashape model of the test pit, including com-

ponent photo set (https://doi.org/10.5683/SP3/CJYTXW), the site-specific safety plan (in French; https://doi.org/10.5683/SP3/AQJKYT), a photo gallery of the expression of the scarp in the field (https://doi.org/10.5683/SP3/6PJ8E8) the complete ambient noise spectra collected at 21 sites (https://doi.org/10.5683/SP3/MFSRWQ), seismic refraction profile and dataset (https://doi.org/10.5683/SP3/GTPCZ1), and the GPR dataset (https://doi.org/10.5683/SP3/FPDSOE).

Competing interests

The authors declare no conflict of interest.

References

Acerra, C., Aguacil, G., Anastasiadis, A., Atakan, K., Azzara, R., Bard, P.-Y., Basili, R., Bertrand, E., Bettig, B., Blarel, F., et al. Guidelines for the implementation of the H/V spectral ratio technique on ambient vibrations measurements, processing and interpretation. *European Commission–EVG1-CT-2000-00026 SESAME*, 2004.

Adams, J., Wetmiller, R. J., Hasegawa, H. S., and Drysdale, J. The first surface faulting from a historical intraplate earthquake in North America. *Nature*, 352:617–619, 1991. doi: 10.1038/352617a0.

Akçiz, S. O., Ludwig, L. G., Zielke, O., and Arrowsmith, J. R. Three-dimensional investigation of a 5 m deflected swale along the San Andreas fault in the Carrizo Plain. *Bulletin of the Seismological Society of America*, 104(6):2799–2808, 2014. doi: https://doi.org/10.1785/0120120172.

Atkinson, G. M. Challenges in seismic hazard analysis for continental interiors. In Stein, S. and Mazzotti, S., editors, *Continental Intraplate Earthquakes: Science, Hazard, and Policy Issues: Geological Society of America Special Paper 425*, page 329–344. The Geological Society of America, 2007. doi: 10.1130/2007.2425(21).

Balsamo, F., Aldega, L., De Paola, N., Faoro, I., and Storti, F. The signature and mechanics of earthquake ruptures along shallow creeping faults in poorly lithified sediments. *Geology*, 42(5): 435–438, 2014. doi: https://doi.org/10.1130/G35272.1.

Basham, P. *New Probabilistic Strong Seismic Ground Motion map of Canada: a Compilation of Earthquake Source Zones, Methods and Results*, volume 82-33. Earth Physics Branch, 1982.

Bennett, M. M. and Glasser, N. F. *Glacial geology: ice sheets and landforms*. John Wiley & Sons, 2011.

Biasi, G. P. and Weldon, R. J. Estimating surface rupture length and magnitude of paleoearthquakes from point measurements of rupture displacement. *Bulletin of the Seismological Society of America*, 96(5):1612–1623, 2006.

Bray, J. D., Seed, R. B., Ciuff, L. S., and Seed, H. B. Earthquake fault rupture propagation through soil. *Journal of Geotechnical Engineering*, 120(3):543–561, 1994. doi: https://doi.org/10.1061/(ASCE)0733-9410(1994)120:3(543).

Brooks, G. R. and Adams, J. A review of evidence of glacially-induced faulting and seismic shaking in eastern Canada. *Quaternary Science Reviews*, 228:106070, 2020. doi: https://doi.org/10.1016/j.quascirev.2019.106070.

Brooks, G. R. and Perret, D. A long-term context for the 1663 Charlevoix CE earthquake interpreted from the postglacial landslide record in the Gouffre Valley, Quebec, Canada. *Quaternary Science Reviews*, 309:108096, 2023. doi: https://doi.org/10.1016/j.quascirev.2023.108096.

Brune, J. N. Precariously balanced rocks and ground-motion maps for southern California. *Bulletin of the Seismological Society of America*, 86(1A):43–54, 1996.

Chien, J. and Liu, Y. Application of a Novel Workflow to Enhance Seismicity Catalog and Compute Earthquake Source Parameters in the Western Québec Seismic Zone. In *American Geophysical Union Fall Meeting; presentation S21E-0339, San Francisco, USA*, 2023. https://agu.confex.com/agu/fm23/meetingapp.cgi/Paper/1387806.

Cox, S. C., Stirling, M. W., Herman, F., Gerstenberger, M., and Ristau, J. Potentially active faults in the rapidly eroding landscape adjacent to the Alpine Fault, central Southern Alps, New Zealand. *Tectonics*, 31(2), 2012. doi: https://doi.org/10.1029/2011TC003038.

Cronin, T. M., Manley, P. L., Brachfeld, S., Manley, T., Willard, D., Guilbault, J.-P., Rayburn, J. A., Thunell, R., and Berke, M. Impacts of post-glacial lake drainage events and revised chronology of the Champlain Sea episode 13–9 ka. *Palaeogeography, Palaeoclimatology, Palaeoecology*, 262(1-2):46–60, 2008. doi: https://doi.org/10.1016/j.palaeo.2008.02.001.

Doig, R. 2300 yr history of seismicity from silting events, in Lake Tadoussac, Charlevoix, Quebec. *Geology*, 18 (9):820–823, 1990. doi: https://doi.org/10.1130/0091-7613(1990)018<0820:YHOSFS>2.3.CO;2.

Dyke, A., Andrews, J., Clark, P., England, J., Miller, G., Shaw, J., and Veillette, J. The Laurentide and Innuitian ice sheets during the last glacial maximum. *Quaternary Science Reviews*, 21(1-3): 9–31, 2002. doi: https://doi.org/10.1016/S0277-3791(01)00095-6.

Earthquakes Canada. 2020 National Building Code of Canada seismic hazard maps. Technical Report Article 1.1.3.1 of Division B, Government of Canada, 2020. Retrieved October 2023 from https://earthquakescanada.nrcan.gc.ca/hazard-alea/zoning-zonage/NBCC2020maps-en.php.

Ebel, J. E. A new analysis of the magnitude of the February 1663 earthquake at Charlevoix, Quebec. *Bulletin of the Seismological Society of America*, 101(3):1024–1038, 2011. doi: https://doi.org/10.1785/0120100190.

Fenton, C. H., Adams, J., and Halchuk, S. Seismic hazards assessment for radioactive waste disposal sites in regions of low seismic activity. *Geotechnical & Geological Engineering*, 24:579–592, 2006. doi: https://doi.org/10.1007/s10706-005-1148-4.

Figueiredo, P., Hill, J., Merschat, A., Scheip, C., Stewart, K., Owen, L., Wooten, R., Carter, M., Szymanski, E., Horton, S., et al. The Mw 5.1, 9 August 2020, Sparta earthquake, North Carolina: The first documented seismic surface rupture in the eastern United States. *GSA Today*, 32(3-4), 2022. doi: https://doi.org/10.1130/GSATG517A.1. CC-BY-NC.

Globensky, Y. Géologie des basses-terres du Saint-Laurent. Technical Report MM 85-02, Les publications du Ministère de l'Énergie et des Ressources Naturelles Québec, 1987.

Godbout, P.-M., Brouard, E., and Roy, M. 1-km resolution rebound surfaces and paleotopography of glaciated North America since the Last Glacial Maximum. *Scientific Data*, 10(1):735, 2023. doi: https://doi.org/10.1038/s41597-023-02566-5.

Goudarzi, M. A. *GPS inferred velocity and strain rate fields in eastern Canada*. PhD thesis, Université Laval, 2016.

Gourdeau, A., Prush, V., Rowe, C. D., Wang, K., Laly, M., Rosset, P., Chouinard, L., Lamothe, M., Nackers, I. M. C., and Mark, H. An Ongoing Search for Active Faults in the Western Quebec Seismic Zone, Eastern Canada. In *American Geophysical Union Fall Meeting; presentation T11D-0188, San Francisco, USA*, 2023. https://agu.confex.com/agu/fm23/meetingapp.cgi/Paper/1365245.

Gouvernement du Québec. Code de sécurité pour les

travaux de construction en date du 1er Juillet 2023, Loi sur la santé et la sécurité du travail, chapitre S-2.1, a. 223, section III : Chantiers de construction (3.15.3.), 1979. https://www.legisquebec.gouv.qc.ca/fr/document/lc/S-2.1?langCont=en#se:223. Accessed 2023-07-01 from https://www.legisquebec.gouv.qc.ca/fr/document/lc/S-2.1?langCont=en#se:223.

Grasemann, B., Martel, S., and Passchier, C. Reverse and normal drag along a fault. *Journal of Structural Geology*, 27(6): 999–1010, 2005. doi: 10.1016/J.JSG.2005.04.006.

Guedes, V. J. C. B., Maciel, S. T. R., and Rocha, M. P. Refrapy: A Python program for seismic refraction data analysis. *Computers & Geosciences*, 159:105020, 2022. doi: https://doi.org/10.1016/j.cageo.2021.105020.

Henton, J. A., Craymer, M. R., Ferland, R., Dragert, H., Mazzotti, S., and Forbes, D. L. Crustal motion and deformation monitoring of the Canadian landmass. *Geomatica*, 60(2):173–191, 2006. doi: https://doi.org/10.5623/geomat-2006-0021.

Hersi, O. S., Lavoie, D., and Nowlan, G. Reappraisal of the Beekmantown Group sedimentology and stratigraphy, Montréal area, southwestern Quebec: implications for understanding the depositional evolution of the Lower–Middle Ordovician Laurentian passive margin of eastern Canada. *Canadian Journal of Earth Sciences*, 40(2):149–176, 2003. doi: https://doi.org/10.1139/e02-077.

Hoque, M. Géologie du Québec: Introduction. Technical Report MM 94-01, Les publications du Ministère de l'Énergie et des Ressources Naturelles Québec, 2014.

Hu, G., Zeng-Liu, J., Shao, Y., Qin, K., and Gao, Y. The applications of optically stimulated luminescence dating in active fault and paleo-earthquake studies: A review. *Quaternary International*, 2024. doi: https://doi.org/10.1016/j.quaint.2024.01.016.

Iturrieta, P., Gerstenberger, M. C., Rollins, C., Van Dissen, R., Wang, T., and Schorlemmer, D. Accounting for the variability of earthquake rates within low-seismicity regions: Application to the 2022 Aotearoa New Zealand National Seismic Hazard Model. *Bulletin of the Seismological Society of America*, 114(1):217–243, 2024. doi: https://doi.org/10.1785/0120230164.

Kozacı, Ö., Madugo, C. M., Bachhuber, J. L., Hitchcock, C. S., Kottke, A. R., Higgins, K., Wade, A., and Rittenour, T. Rapid postearthquake field reconnaissance, paleoseismic trenching, and GIS-based fault slip variability measurements along the Mw 6.4 and Mw 7.1 Ridgecrest earthquake sequence, southern California. *Bulletin of the Seismological Society of America*, 111(5): 2334–2357, 2021. doi: https://doi.org/10.1785/0120200262.

Kumarapeli, P. and Saull, V. A. The St. Lawrence valley system: a North American equivalent of the East African rift valley system. *Canadian Journal of Earth Sciences*, 3(5):639–658, 1966. doi: https://doi.org/10.1139/e66-045.

Lambeck, K., Purcell, A., and Zhao, S. The North American Late Wisconsin ice sheet and mantle viscosity from glacial rebound analyses. *Quaternary Science Reviews*, 158:172–210, 2017. doi: https://doi.org/10.1016/j.quascirev.2016.11.033.

Lamontagne, M. An overview of some significant eastern Canadian earthquakes and their impacts on the geological environment, buildings and the public. *Natural hazards*, 26:55–68, 2002. doi: https://doi.org/10.1023/A:1015268710302.

Lamontagne, M., Halchuk, S., Cassidy, J. F., and Rogers, G. C. *Significant Canadian Earthquakes 1600-2017*. Geological Survey of Canada, 2018.

Lamothe, M. Géologie des formations quaternaires de la région du Lac Saint-Pierre. Technical report, Rapport Statutaire Intragaz, Min Ress Nat Québec, 1993.

Leblanc, G. A closer look at the September 16, 1732, Montreal earthquake. *Canadian Journal of Earth Sciences*, 18(3):539–550, 1981. doi: https://doi.org/10.1139/e81-047.

Leonard, M. Self-consistent earthquake fault-scaling relations: Update and extension to stable continental strike-slip faults. *Bulletin of the Seismological Society of America*, 104(6):2953–2965, 2014.

Ma, S. and Eaton, D. W. Western Quebec seismic zone (Canada): Clustered, midcrustal seismicity along a Mesozoic hot spot track. *Journal of Geophysical Research: Solid Earth*, 112(B6), 2007. doi: https://doi.org/10.1029/2006JB004827.

Markovaara-Koivisto, M., Ojala, A. E., Mattila, J., Kukkonen, I., Aro, I., Pullinen, A., Hänninen, P., Middleton, M., Sutinen, A., Majaniemi, J., et al. Geomorphological evidence of paleoseismicity: surficial and underground structures of Pasmajärvi postglacial fault. *Earth Surface Processes and Landforms*, 45(12): 3011–3024, 2020. doi: https://doi.org/10.1002/esp.4948.

Mazzotti, S. Geodynamic models for earthquake studies in intraplate North America. In Stein, S. and Mazzotti, S., editors, *Continental Intraplate Earthquakes: Science, Hazard, and Policy Issues*, volume 425 of *Geological Society of America Special Papers*, pages 17–33. The Geological Society of America, 2007. doi: https://doi.org/10.1130/2007.2425(02).

McCalpin, J., editor. *Paleoseismology, 2nd Edition*. Elsevier Academic Press, 2009.

Mérindol, M., St-Onge, G., Sultan, N., Lajeunesse, P., and Garziglia, S. Earthquake-triggered submarine landslides in the St. Lawrence Estuary (Québec, Canada) during the last two millennia and the record of the major 1663 CE M$\geq$ 7 event. *Quaternary Science Reviews*, 291:107640, 2022. doi: https://doi.org/10.1016/j.quascirev.2022.107640.

Mikko, H., Smith, C. A., Lund, B., Ask, M. V., and Munier, R. LiDAR-derived inventory of post-glacial fault scarps in Sweden. *GFF*, 137(4):334–338, 2015. doi: https://doi.org/10.1080/11035897.2015.1036360.

Ministère de l'Économie, de l'Innovation et de l'Énergie. Démographie, population, 2022. https://www.economie.gouv.qc.ca/pages-regionales/montreal/portrait-regional/demographie, retrieved 17 July 2023.

Ministère des Forêts, Faune et Parcs, Q. P. D. Q. LiDAR - Modèles Numériques (terrain, canopée, pente). https://www.donneesquebec.ca/recherche/fr/dataset/produits-derives-de-base-du-lidar, 2016.

Ministère des Ressources naturelles et des Forêts. système d'information géominière, Carte interactive. Technical report, Gouvernement du Québec, 2021. Quebec Geomining Information System retrieved on January 22 2024 from https://sigeom.mines.gouv.qc.ca/signet/classes/I1108_afchCarteIntr.

Molnar, S., Cassidy, J., Castellaro, S., Cornou, C., Crow, H., Hunter, J., Matsushima, S., Sánchez-Sesma, F., and Yong, A. Application of microtremor horizontal-to-vertical spectral ratio (MHVSR) analysis for site characterization: State of the art. *Surveys in Geophysics*, 39:613–631, 2018. doi: https://doi.org/10.1007/s10712-018-9464-4.

Morell, K. D., Styron, R., Stirling, M., Griffin, J., Archuleta, R., and Onur, T. Seismic hazard analyses from geologic and geomorphic data: Current and future challenges. *Tectonics*, 39(10):e2018TC005365, 2020. doi: https://doi.org/10.1029/2018TC005365.

Mörner, N.-A., Tröften, P. E., Sjöberg, R., Grant, D., Dawson, S., Bronge, C., Kvamsdal, O., and Sidén, A. Deglacial paleoseismicity in Sweden: the 9663 BP Iggesund event. *Quaternary Science Reviews*, 19(14-15):1461–1468, 2000. doi: https://doi.org/10.1016/S0277-3791(00)00095-0.

Natural Resources Canada. Earthquakes Database, search the Earthquake Database. https://www.earthquakescanada.nrcan.gc.ca/stndon/NEDB-BNDS/bulletin-en.php, 2024. Accessed 6 June 2024.

Occhietti, S. and Richard, P. J. Effet réservoir sur les âges ^{14}C de la Mer de Champlain à la transition Pléistocène-Holocène: révision de la chronologie de la déglaciation au Québec méridional. *Géographie physique et Quaternaire*, 57(2):115–138, 2003. doi: https://doi.org/10.7202/011308ar.

Occhietti, S., Parent, M., Lajeunesse, P., Robert, F., and Govare, É. Late Pleistocene–early Holocene decay of the Laurentide ice sheet in Québec–Labrador. In *Developments in quaternary sciences*, volume 15, pages 601–630. Elsevier, 2011. doi: https://doi.org/10.1016/B978-0-444-53447-7.00047-7.

Oettle, N. K. and Bray, J. D. Fault rupture propagation through previously ruptured soil. *Journal of Geotechnical and Geoenvironmental Engineering*, 139(10):1637–1647, 2013. doi: https://doi.org/10.1061/(ASCE)GT.1943-5606.0000919.

Oliver, J., Johnson, T., and Dorman, J. Postglacial faulting and seismicity in New York and Quebec. *Canadian Journal of Earth Sciences*, 7(2):579–590, 1970. doi: https://doi.org/10.1139/e70-059.

Pagani, M., Monelli, D., Weatherill, G., Danciu, L., Crowley, H., Silva, V., Henshaw, P., Butler, L., Nastasi, M., Panzeri, L., et al. OpenQuake engine: An open hazard (and risk) software for the global earthquake model. *Seismological Research Letters*, 85(3): 692–702, 2014. doi: https://doi.org/10.1785/0220130087.

Palmu, J.-P., Ojala, A. E., Ruskeeniemi, T., Sutinen, R., and Mattila, J. LiDAR DEM detection and classification of postglacial faults and seismically-induced landforms in Finland: a paleoseismic database. *Gff*, 137(4):344–352, 2015. doi: https://doi.org/10.1080/11035897.2015.1068370.

Pinet, N., Lamontagne, M., Duchesne, M. J., and Brake, V. I. Hunting for Quaternary faults in eastern Canada: A critical appraisal of two potential candidates. *Seismological Research Letters*, 92 (2A):1102–1111, 12 2020. doi: 10.1785/0220200322.

Pisarska-Jamroży, M., Belzyt, S., Bitinas, A., Jusienė, A., and Woronko, B. Seismic shocks, periglacial conditions and glaciotectonics as causes of the deformation of a Pleistocene meandering river succession in central Lithuania. *Baltica*, 32(1): 63–77, 2019. doi: https://doi.org/10.5200/baltica.2019.1.6.

Randour, I., Daigneault, R.-A., Lamothe, M., Roy, M., and Robitaille, A. Région des Laurentides. Technical Report MB202008PLAN006, Ministère des Ressources naturelles et des Forêts, 2020a. https://gq.mines.gouv.qc.ca/documents/EXAMINE/MB202008/MB202008PLAN001.pdf.

Randour, I., Daigneault, R.-A., Lamothe, M., Roy, M., and Robitaille, A. Cartographie des formations superficielles de la région des Laurentides-Lanaudière, phase 2. *Gouvernement du Québec, Canada*, 2020b.

Richard, P. J. and Occhietti, S. 14C chronology for ice retreat and inception of Champlain Sea in the St. Lawrence Lowlands, Canada. *Quaternary Research*, 63(3):353–358, 2005. doi: https://doi.org/10.1016/j.yqres.2005.02.003.

Rimando, J. M. and Peace, A. L. Reactivation potential of intraplate faults in the western Quebec seismic zone, eastern Canada. *Earth and Space Science*, 8(8):e2021EA001825, 2021. doi: https://doi.org/10.1029/2021EA001825.

Roesset, J. Fundamentals of soil amplification. In Hansen, R., editor, *Seismic Design for Nuclear Power Plants*, page 183–244. M.I.T. Press, 1970.

Rood, A., Rood, D., Stirling, M., Madugo, C., Abrahamson, N., Wilcken, K., Gonzalez, T., Kottke, A., Whittaker, A., Page, W., et al. Earthquake hazard uncertainties improved using precariously balanced rocks. *AGU Advances*, 1(4):e2020AV000182, 2020. doi: https://doi.org/10.1029/2020AV000182.

Rosset, P., Bour-Belvaux, M., , and Chouinard, L. Estimation and comparison of Vs30; microzonation maps for Montreal Using multiple sources of information. *Bulletin of Earthquake Engineering*, 13(8):2225–2239, 2015. doi: https://doi.org/10.3390/geosciences13090256.

Rosset, P., Chouinard, L., and Nollet, M.-J. Consequences on residential buildings in greater Montreal for a repeat of the 1732 M5.8 Montreal earthquake. In *Canadian Society of Civil Engineering Annual Conference*, pages 667–679. Springer, 2021. doi: https://doi.org/10.1007/978-981-19-0507-0_58.

Rosset, P., Long, X., and Chouinard, L. Influence of the 2020 Seismic Hazard Update on residential losses in greater Montreal, Canada. *GeoHazards*, 4(4):406–420, 2023. doi: https://doi.org/10.3390/geohazards4040023.

Rücker, C., Günther, T., and Wagner, F. M. pyGIMLi: An open-source library for modelling and inversion in geophysics. *Computers & Geosciences*, 109:106–123, 2017. doi: https://doi.org/10.1016/j.cageo.2017.07.011.

Sella, G. F., Stein, S., Dixon, T. H., Craymer, M., James, T. S., Mazzotti, S., and Dokka, R. K. Observation of glacial isostatic adjustment in "stable" North America with GPS. *Geophysical Research Letters*, 34(2), 2007. doi: https://doi.org/10.1029/2006GL027081.

Shilts, W. W. Sangamonian and early Wisconsinan events in the St. Lawrence Lowland and Appalachians of southern Quebec, Canada. *The last interglacial-glacial transition in North America*, 270:171, 1992. doi: https://doi.org/10.1130/SPE270-p171.

Simon, K., James, T., Henton, J., and Dyke, A. A glacial isostatic adjustment model for the central and northern Laurentide Ice Sheet based on relative sea level and GPS measurements. *Geophysical Journal International*, 205(3):1618–1636, 2016. doi: https://doi.org/10.1093/gji/ggw103.

Smith, C. A., Sundh, M., and Mikko, H. Surficial geology indicates early Holocene faulting and seismicity, central Sweden. *International Journal of Earth Sciences*, 103:1711–1724, 2014. doi: https://doi.org/10.1007/s00531-014-1025-6.

St-Onge, G., Mulder, T., Piper, D. J., Hillaire-Marcel, C., and Stoner, J. S. Earthquake and flood-induced turbidites in the Saguenay Fjord (Québec): a Holocene paleoseismicity record. *Quaternary Science Reviews*, 23(3-4):283–294, 2004. doi: https://doi.org/10.1016/j.quascirev.2003.03.001.

Steffen, H., Olesen, O., and Sutinen, R., editors. *Glacially-triggered faulting*. Cambridge University Press, 2021a. doi: https://doi-org.proxy3.library.mcgill.ca/10.1017/9781108779906.

Steffen, R., Wu, P., and Lund, B. Geomechanics of Glacially Triggered Faulting. In *Glacially-Triggered Faulting*. Cambridge University Press, 2021b. doi: https://doi.org/10.1017/9781108779906.004.

Stein, S. Approaches to continental intraplate earthquake issues. In Stein, S. and Mazzotti, S., editors, *Continental Intraplate Earthquakes: Science, Hazard, and Policy Issues: Geological Society of America Special Paper*, volume 425, page 1–16. Geological Society of America, 2007. doi: https://doi.org/10.1130/SPE425.

Stevens, V. and Avouac, J. On the relationship between strain rate and seismicity in the India–Asia collision zone: implications for probabilistic seismic hazard. *Geophysical Journal International*, 226(1):220–245, 2021. doi: https://doi.org/10.1093/gji/ggab098.

Sutinen, R., Hyvönen, E., Middleton, M., and Ruskeeniemi, T. Airborne LiDAR detection of postglacial faults and Pulju moraine in Palojärvi, Finnish Lapland. *Global and Planetary*

Change, 115:24–32, 2014. doi: https://doi.org/10.1016/j.gloplacha.2014.01.007.

Tarayoun, A., Mazzotti, S., Craymer, M., and Henton, J. Structural inheritance control on intraplate present-day deformation: GPS strain rate variations in the Saint Lawrence Valley, eastern Canada. *Journal of Geophysical Research: Solid Earth*, 123(8): 7004–7020, 2018. doi: https://doi.org/10.1029/2017JB015417.

Thompson Jobe, J., Hatem, A., Gold, R., DuRoss, C., Reitman, N., Briggs, R., and Collett, C. Earthquake geology inputs for the National Seismic Hazard Model (NSHM) 2023 (central and eastern United States), version 1.0. Technical report, U.S. Geological Survey data release, https://doi.org/10.5066/P94HLE5G., 2022.

Tremblay, A., Roden-Tice, M. K., Brandt, J. A., and Megan, T. W. Mesozoic fault reactivation along the St. Lawrence rift system, eastern Canada: Thermochronologic evidence from apatite fission-track dating. *Bulletin*, 125(5-6):794–810, 2013. doi: https://doi.org/10.1130/B30703.1.

Tuttle, M. and Seeber, L. Historic and prehistoric earthquake-induced liquefaction in Newbury, Massachusetts. *Geology*, 19(6):594–597, 1991. doi: https://doi.org/10.1130/0091-7613(1991)019<0594:HAPEIL>2.3.CO;2.

Tuttle, M. P. and Atkinson, G. M. Localization of large earthquakes in the Charlevoix seismic zone, Quebec, Canada, during the past 10,000 years. *Seismological Research Letters*, 81(1):140–147, 2010. doi: https://doi.org/10.1785/gssrl.81.1.140.

Vrolijk, P., Pevear, D., Covey, M., and LaRiviere, A. Fault gouge dating: history and evolution. *Clay Minerals*, 53(3):305–324, 2018. doi: https://doi.org/10.1180/clm.2018.22.

Walcott, R. Late Quaternary vertical movements in eastern North America: Quantitative evidence of glacio-isostatic rebound. *Reviews of Geophysics*, 10(4):849–884, 1972. doi: https://doi.org/10.1029/RG010i004p00849.

Wathelet, M., Chatelain, J.-L., Cornou, C., Giulio, G. D., Guillier, B., Ohrnberger, M., and Savvaidis, A. Geopsy: A user-friendly open-source tool set for ambient vibration processing. *Seismological Research Letters*, 91(3):1878–1889, 2020. doi: https://doi.org/10.1785/0220190360.

Weichert, D. Omak rock and the 1872 Pacific Northwest earthquake. *Bulletin of the Seismological Society of America*, 84(2): 444–450, 1994.

Wells, D. and Coppersmith, K. Likelihood of surface rupture as a function of magnitude. *Seismological Research Letters*, 64(1): 54, 1993.

Yu, H., Liu, Y., Harrington, R. M., and Lamontagne, M. Seismicity along St. Lawrence Paleorift faults overprinted by a meteorite impact structure in Charlevoix, Québec, Eastern Canada. *Bulletin of the Seismological Society of America*, 106(6):2663–2673, 2016. doi: https://doi.org/10.1785/0120160036.

Zelt, C. A. Lateral velocity resolution from three-dimensional seismic refraction data. *Geophysical Journal International*, 135(3):1101–1112, 1998. doi: https://doi.org/10.1046/j.1365-246X.1998.00695.x.

Zielke, O., Klinger, Y., and Arrowsmith, J. R. Fault slip and earthquake recurrence along strike-slip faults—Contributions of high-resolution geomorphic data. *Tectonophysics*, 638:43–62, 2015. doi: https://doi.org/10.1016/j.tecto.2014.11.004.